arXiv:1304.2511v1 [cond-mat.soft] 9 Apr 2013

Consistent coarse-graining strategy for polymer solutions in the thermal crossover from good to θ solvent.

Giuseppe D'Adamo*
Dipartimento di Fisica, Sapienza Università di Roma, P.le Aldo Moro 2, I-00185 Roma, Italy

Andrea Pelissetto†
Dipartimento di Fisica, Sapienza Università di Roma and INFN, Sezione di Roma I, P.le Aldo Moro 2, I-00185 Roma, Italy

Carlo Pierleoni‡
Dipartimento di Scienze Fisiche e Chimiche, Università dell'Aquila and CNISM, UdR dell'Aquila, V. Vetoio 10, Loc. Coppito, I-67100 L'Aquila, Italy

(Dated: April 10, 2013)

We extend our previously developed coarse-graining strategy for linear polymers with a tunable number n of effective atoms (blobs) per chain [D'Adamo *et al.*, J. Chem. Phys. **137**, 4901 (2012)] to polymer systems in thermal crossover between the good-solvent and the θ regimes. We consider the thermal crossover in the region in which tricritical effects can be neglected, i.e., not too close to the θ point, for a wide range of chain volume fractions $\Phi = c/c^*$ (c^* is the overlap concentration), up to $\Phi \approx 30$. Scaling crossover functions for global properties of the solution are obtained by Monte Carlo simulations of the Domb-Joyce model with suitably rescaled on-site repulsion. They provide the input data to develop a minimal coarse-grained model with four blobs per chain (tetramer model). As in the good-solvent case, the coarse-grained model potentials are derived at zero density, thus avoiding the inconsistencies related to the use of state-dependent potentials. We find that the coarse-grained model reproduces the properties of the underlying, full-monomer system up to some reduced density Φ which increases when lowering the temperature towards the θ state. Close to the lower-temperature crossover boundary, the tetramer model is accurate at least up to $\Phi \simeq 10$, while near the good-solvent regime reasonably accurate results are obtained up to $\Phi \simeq 2$. The density region in which the coarse-grained model is predictive can be enlarged by developing coarse-grained models with more blobs per chain. We extend the strategy used in the good-solvent case to the crossover regime. This requires a proper treatment of the length rescalings as before, but also a proper temperature redefinition as the number of blobs is increased. The case $n = 10$ is investigated in detail. We obtain the potentials for such finer-grained model starting from the tetramer ones. Comparison with full-monomer results shows that the density region in which accurate predictions can be obtained is significantly wider than that corresponding to the tetramer case.

PACS numbers: 61.25.he, 65.20.De, 82.35.Lr

I. INTRODUCTION

The phase diagram of solutions of linear polymers and their large-scale structure (i.e., on the scale of the coil size) are well understood and can be explained by invoking the physical picture of polymers in implicit solvent with effective (solvent-mediated) interactions among the monomers.[1–5] When the number L of monomers per chain (degree of polymerization) is large, such chains exhibit scale invariance, meaning that, in suitably rescaled units of density, temperature, and chain length, solutions of chemically distinct polymers and solvents obey universal scaling relations, i.e., global properties of the solution are characterized by *universal* exponents and scaling functions. Central properties are the single-chain radius of gyration R_g and the equation of state for the osmotic pressure Π. For small concentrations, Π admits the expansion[6]

$$Z = \frac{\beta\Pi}{c} = 1 + B_2 c + B_3 c^2 + o(c^3), \qquad (1)$$

where $\beta = 1/(k_B T)$, B_k are the usual virial coefficients, and $c = N/V$ is the polymer density (N chains in a volume V). The coefficients B_k depend on all chemical details. On the other hand, the dimensionless ratios $A_k = B_k \hat{R}_g^{-3(k-1)}$ ($\hat{R}_g$ is the zero-density radius of gyration) have a universal limit, i.e., they are independent of chemical details, for large values of L.

Scaling functions and exponents are influenced by the nature of the interactions among the monomers. Three regimes can be distinguished.[7] i) The *good-solvent* regime, usually observed at high enough temperature, in which interactions are dominated by the pairwise repulsion and the single-chain size grows[1,8] as L^ν, where[9] $\nu = 0.587597(7) \simeq 3/5$ is the Flory exponent. The second virial coefficient is positive and[10] $A_2 = 5.500(3)$ for $L \to \infty$. ii) The *θ-regime* at lower temperature, in which the repulsive and attractive contributions in the two-body and three-body effective interactions are vanishingly small and of the same order of magnitude. In the scaling limit $L \to \infty$, this regime collapses to a single temperature T_θ, called θ temperature. At $T = T_\theta$ chains

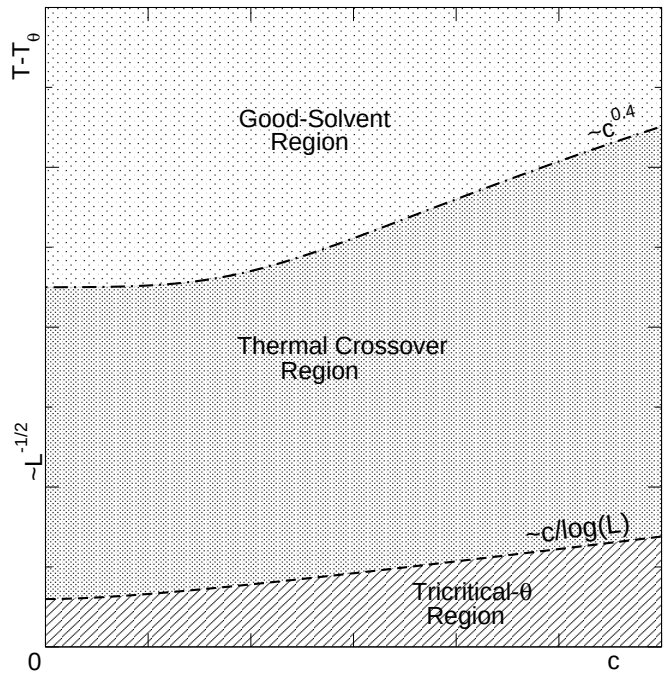

FIG. 1: Temperature(T)-concentration(c) phase diagram for solutions of polymers of finite length L.

are Gaussian (ideal) with scaling exponent $\nu = 1/2$ and the second virial combination A_2 vanishes. However, for linear chains of finite length, as is the case in experiments and computer simulations, this regime is observed in a temperature interval around T_θ of the order of $1/\sqrt{L}$. In analogy with the dilute-gas case, one often defines the "Boyle" temperature T_B, as the value of T at which the second virial coefficient B_2 vanishes. T_B is generally larger then T_θ, converges to T_θ as $L \to \infty$ [$T_B = T_\theta + O(L^{-1/2}(\ln L)^{-7/11})$], and is sometimes used to estimate T_θ numerically.[11] iii) At even lower temperatures the two-body effective interactions become predominantly attractive (negative second virial coefficient), the chains are segregated by the solvent and below a critical temperature T_c the solution separates in a chain-poor solution where chains are in the collapsed state, and a solvent-poor solution where the chain statistics approaches the one in the melt state (ideal at large scales). Again, in the scaling limit $L \to \infty$ the critical temperature T_c tends to T_θ.[2–4]

For finite values of L, a gradual transition between the good- and θ-solvent regimes is observed, i.e., the observables and their associated scaling functions interpolate smoothly between the two universal behaviors. A sketch of the various regimes in the phase diagram of polymers of finite length is shown in Figure 1. At low polymer concentration, i.e., for $\Phi \ll 1$, when increasing the temperature above the θ point, the coil size is observed to behave as L^ν with an apparent exponent that increases from 1/2 to 3/5. Analogously, the second virial combination A_2 varies smoothly in the range $0 \le A_2 \le 5.5$, with the value 5.5 (plus finite L corrections) obtained in the fully developed good-solvent regime.[10] At larger polymer concentrations and for any $T \ge T_\Theta$, a region where 2-body and 3-body terms are of the same order of magnitude is present and is generically referred as *tricritical region*. For small concentrations this region extends in a small temperature interval[2,7] whose width is of the order of $1/\sqrt{L}$ (more precisely, it scales as $L^{-1/2}(\ln L)^{-7/11}$). As the concentration c increases, this region widens as $c/\ln L$. In the tricritical region scaling corrections decay very slowly, as inverse powers of $\log L$.[4,5,12,13] Outside the tricritical region the physics is again dominated by two-body effects and by the unbalance between the short-range repulsion and the long-range attraction, as it was shown by computer simulations of physical polymer models.[14] Here we refer to the *thermal crossover region*, as the region in the phase diagram between the tricritical and good-solvent regimes. At finite concentration, scaling arguments[15] indicate that the size of the thermal crossover region grows with c as $c^{1/(6\nu-2)} \sim c^{0.40}$. At sufficiently large temperatures, the good-solvent regime is reached at any concentration.

In the thermal crossover region there are experimental and computer-simulation evidences that, for sufficiently large values of L, global properties of the solution follow, up to small corrections in T, Φ, and L, general relations of the form

$$\mathcal{O}(T, c, L) = \alpha_1 \mathcal{O}_G(L, c) f_{\mathcal{O}}(z, \Phi), \qquad (2)$$

where $\mathcal{O}_G(L, c)$ is the expression of $\mathcal{O}$ for the Gaussian chain, the function $f_{\mathcal{O}}$ is called *crossover* function, $z = \alpha_2(T - T_\theta)L^{1/2}$, and α_1 and α_2 are nonuniversal constants that embody all chemical details. Theory[4,5,12] supports the scaling behavior (2), albeit with a slightly different scaling variable. Indeed, the crossover limit should be taken by keeping $\alpha_2(T - T_\theta)L^{1/2}(\ln L)^{-4/11}$ fixed, which differs by a power of $\ln L$ from the scaling variable $z = (T - T_\theta)L^{1/2}$ which appears in Eq. (2). Such a logarithmic dependence is irrelevant in all practical applications, since the observation of this slowly varying term would require data in a very large interval of polymer lengths/molecular weights. By varying z one obtains the full crossover behavior, from the tricritical region, corresponding to small values of z, to the good-solvent regime, which is obtained for $z \to \infty$.

It is important to note that the nontrivial universal behavior is obtained when taking simultaneously the limits $L \to \infty$ and $T \to T_\theta$ in such a way that the arguments of the crossover function $f_{\mathcal{O}}$, $z \equiv \alpha_2(T - T_\theta)L^{1/2}$ and Φ, remain constant. If the limits are taken differently, one would obtain a different result. For instance, if one takes the limit $L \to \infty$ at fixed $T > T_\theta$, one would obtain good-solvent behavior in all cases, while, if one decreases T towards T_θ at fixed large L, only the tricritical behavior would be observed. A similar variety of universal scaling behaviors, which depend on how the limit $L \to \infty$ is taken, is found in the stretched-chain problem.[16]

The variable z that parametrizes the temperature crossover depends on the nonuniversal parameter α_2, hence a proper definition requires specifying a physically meaningful normalization condition. To avoid this problem, one can proceed as suggested in Refs. 14,17, i.e., one can parametrize the crossover in terms of a physical variable rather than in terms of z. For instance, one can use the dimensionless second-virial combination A_2. Then, Eq. (2) can be written as

$$\mathcal{O}(T, L, c) = \alpha_1 \mathcal{O}_G(L, c) g_{\mathcal{O}}(A_2, \Phi), \tag{3}$$

where $g_{\mathcal{O}}(A_2, \Phi)$ is universal. The *quality* of the solution is now characterized by A_2 that varies between zero at the θ point and $A_{2,GS} \simeq 5.5$, the good-solvent value.[10] In the thermal crossover region the relation between z and A_2 has been obtained combining analytical results and Monte Carlo simulations,[15] obtaining

$$A_2(z) = 4\pi^{3/2} z (1 + 19.1187 z + 126.783 z^2 + 331.99 z^3 + 268.96 z^4)^{-1/4}, \tag{4}$$

where z has been normalized so that $A_2(z) \approx 4\pi^{3/2} z$ for small z, i.e., $\Psi(z) \approx z$, where $\Psi = 2(4\pi)^{-3/2} A_2$ is the so-called interpenetration ratio, which is commonly used in much of the experimental literature.

As discussed by Sokal,[18] the universal scaling functions that parametrize the thermal crossover coincide with the crossover functions that are defined in the two-parameters model (TPM),[4,5,19] which considers only repulsive two-body monomer-monomer interactions. In this framework the scaling variable z is identified with the usual Zimm-Stockmayer-Fixmann variable.[20] Therefore, to determine the leading crossover behavior, it is convenient to work in the TPM framework, which provides directly the crossover functions. This is the approach we have taken in this paper, using the lattice Domb-Joyce model,[21] which is the lattice version of the continuum TPM, to obtain the crossover functions, both in the dilute and in the semidilute regime.

Although the physics of homogenous polymer solutions is well understood, in more complex situations—for instance, inhomogeneous cases or when the polymers are only a single component of a more complex system—it might be important to reduce the number of degrees of freedom representing the polymer subsystem or, equivalently, to limit our interest to the physics occurring at a length scale comparable to the polymer size. In these cases adopting a coarse-grained (CG) representation of the solution might be essential for the feasibility of the numerical investigation. Moreover, since the target properties on which the coarse-grained model (CGM) is built can be determined in the scaling limit $L \to \infty$, CGMs allow one to study thermodynamics and structural properties in the universal, scaling limit without requiring additional extrapolations.

Several routes to CGMs can be adopted. In the structure-based route[22–25] the CGM is set up in such a way to reproduce the marginal probability distribution of a set of chosen structural collective variables. This procedure, however, does not predict the correct thermodynamics of the underlying solution. Conversely, a CGM can be defined to match the thermodynamic behavior, but then structural properties are not reproduced correctly.[26] A third method is the force-matching approach (often called multiscale coarse-graining method[27]), in which the state-dependent pairwise potential is determined by requiring the CG system to match the atomistic force on the CG atoms as accurately as possible. Also this method has a structural interpretation:[28] the matching condition is equivalent to require the CG force to satisfy the appropriate Yvon-Born-Green equation that relates the pair and the three-body correlation function. However, no guarantee of reproducing the pair structure and the thermodynamics is provided. The inconsistency between structure and thermodynamics stems from the fact that CGMs neglect multi-body interactions, which would be required to obtain an exact mapping of the microscopic model onto the CGM.

Recently, we have introduced a procedure to set up a hierarchy of CGMs for linear chains in good-solvent conditions which simultaneously reproduce quite accurately structure and thermodynamics of polymer solutions deep into the semidilute regime.[29,30] The minimal model consists in representing each linear chain by a short polyatomic molecule with four CG sites (tetramer). The tetramer potentials are set up at zero density—this allows us to avoid the inconsistencies[31–33] that occur when using state-dependent potentials—by matching the single-chain intramolecular structure and the center-of-mass pair correlation function between two identical chains. The minimal representation (tetramer) has been shown to provide accurate results for the underlying solutions up to $\Phi \simeq 2$.[29] Larger values of Φ can be accessed by increasing the resolution of the CGM, i.e. by increasing the number of effective monomers (blobs) per chain. The effective potentials for these higher-resolution models are obtained by using a simple transferability approach. We assume that the potentials are independent of the number of blobs, as long as all lengths are expressed in terms of the blob radius of gyration. This transferability approximation was shown to be quite accurate[30] and allowed us to obtain accurate thermodynamic and (large-scale) structural results for $\Phi \gg 1$.

In this paper we present the extension of this CG strategy to solutions in the thermal crossover region, defining CGMs with z-dependent potentials that reproduce the polymer crossover functions. We have considered the TPM as the underlying microscopic model, using the lattice Domb-Joyce (DJ) model[21] as reference system. As in the good-solvent case, we first determine the effective interactions for the tetramer case for several values of z in the crossover region, by matching structural properties at zero density. These potentials are then used to define CGMs of higher resolutions, i.e., higher num-

ber of CG sites. The transferability approach is more complex than in the good-solvent case, since one must change at the same time the reference length scale and the scaling variable z. We perform extensive simulations of the CGMs at finite density, both in the dilute and in the semidilute region. The results are then compared with those obtained in full-monomer (FM) simulations and with the field-theory predictions of Ref. 5. We find that the tetramer CGM reproduces very accurately the crossover functions up to $\Phi \approx 30$ (and quite reasonably at all densities) for small values of z. Close to the good-solvent behavior, instead accurate results are obtained up to $\Phi \simeq 2$. Use of the decamer model with $n = 10$ blobs allows one to widen significantly the density region in which the CGM is predictive.

The present work represents an important extension of our previous results, allowing us to consider polymer systems in the thermal crossover regime. In particular, it opens the way to the study of more complex systems like polymer-colloid solutions away from the good-solvent regime and diblock copolymer solutions,[34,35] where each block has different affinity with the solvent.

The paper is organized as follows. In section II we define the DJ model we have adopted and explain how the crossover functions are computed. In section III we present our CG strategy, first illustrating the CG representation (CGR) of the FM chain (section III A) and later presenting our CGM (section III B). Section IV is devoted to the comparison between the results of the CGR of the FM system and of the CGM, first at zero density (section IV A) and then at finite density in the semidilute regime (section IV C). Simulation results are also compared with field-theoretical expressions[5] and large-density predictions obtained by using the random-phase approximation (RPA), which becomes exact for $\Phi \to \infty$. In section V, the transferability of the tetramer potentials to finer resolution models is illustrated and validated against FM predictions. Finally, section VI reports our conclusions. Two appendices are also present. In Appendix A we report the calculation of the blob radius of gyration in the crossover regime, while in Appendix B we summarize the field-theory predictions of Ref. 5. Some numerical details and explicit expressions for the CGM potentials can be found in the supplementary material.[36]

II. CROSSOVER FUNCTIONS FROM MONTE CARLO SIMULATIONS OF THE DOMB-JOYCE MODEL

In order to compute the TPM crossover functions, we consider the three-dimensional lattice Domb-Joyce (DJ) model.[21] In this model the polymer solution is mapped onto N chains of L monomers each on a cubic lattice of linear size M with periodic boundary conditions. Each polymer chain is modelled by a random walk $\{\mathbf{r}_1^{(i)}, \ldots, \mathbf{r}_L^{(i)}\}$ with $|\mathbf{r}_\alpha^{(i)} - \mathbf{r}_{\alpha+1}^{(i)}| = 1$ (we take the lattice spacing as unit of length) and $1 \le i \le N$. The Hamiltonian is given by

$$H = \sum_{i=1}^{N} \sum_{1 \le \alpha < \beta \le L} \delta(\mathbf{r}_\alpha^{(i)}, \mathbf{r}_\beta^{(i)}) + \sum_{1 \le i < j \le N} \sum_{\alpha=1}^{L} \sum_{\beta=1}^{L} \delta(\mathbf{r}_\alpha^{(i)}, \mathbf{r}_\beta^{(j)}), \quad (5)$$

where $\delta(\mathbf{r}, \mathbf{s})$ is the Kronecker delta. Each configuration is weighted by e^{-wH}, where $w > 0$ is a free parameter that plays the role of inverse temperature. This model is similar to the standard lattice self-avoiding walk (SAW) model,[37,38] which is obtained in the limit $w \to +\infty$. For finite positive w intersections are possible although energetically penalized. For any positive w, this model has the same scaling limit as the SAW model[21] and thus allows us to compute the universal scaling functions that are relevant for polymer solutions under good-solvent conditions.

The TPM results in the thermal crossover region can also be derived from simulations of the DJ model. They are obtained[39] by taking the limit $w \to 0$, $L \to \infty$ at fixed $x = wL^{1/2}$. The variable x interpolates between the ideal-chain limit ($x = 0$) and the good-solvent limit ($x = \infty$). Indeed, for $w = 0$ the DJ model is simply the random-walk model, while for any $w \neq 0$ and $L \to \infty$ one always obtains the good-solvent scaling behavior. The variable x is proportional to the variable z that is used in the TPM context. If we normalize z so that $A_2(z) \approx 4\pi^{3/2} z$ for small z as in Eq. (4), we have[39,40]

$$z \equiv \left(\frac{3}{2\pi}\right)^{3/2} w L^{1/2}. \quad (6)$$

As discussed in Ref. 15, the TPM results can be obtained from Monte Carlo simulations of the DJ model by properly extrapolating the numerical results to $L \to \infty$. For each z we consider several chain lengths L_i. For each of them we determine the interaction parameter w_i by using Eq. (6), that is we set $w_i = (2\pi/3)^{3/2} z L_i^{-1/2}$. Simulations of chains of L_i monomers are then performed setting $w = w_i$. Simulation results are then extrapolated to $L \to \infty$, taking into account that corrections are of order $1/\sqrt{L}$.[39,40] If $R(L, z)$ is a dimensionless ratio of two global quantities at zero density (for instance, the second-virial combination A_2), the TPM result $R^*(z)$ is obtained by performing an extrapolation of the form

$$R(L, z) = R^*(z) + \frac{a(z)}{\sqrt{L}} + O(L^{-1} \ln L). \quad (7)$$

Of course, for $z \to \infty$, $R^*(z)$ converges to its universal good-solvent value, which can be obtained by taking the limit $L \to \infty$ at fixed (arbitrary) w.

In this work we often consider adimensional distribution functions $g(\rho; L, z)$ that also depend on the adimensional ratio $\rho = r/\hat{R}_g$. For these properties, the TPM

TABLE I: Values of z considered in this paper. The notation is such that $A_2(z^{(p)}) \approx p$. The estimates of $A_2(z)$ for $z^{(1)}$, $z^{(2)}$, $z^{(3)}$, $z^{(4)}$, and $z^{(5)}$, are the direct MC estimates of Ref. 15; in the other cases we use the interpolation formula (4). In the last column we report $r = A_2(z)/A_{2,GS} = \Psi(z)/\Psi_{GS}$ (Ψ is the interpenetration ratio often used in experimental work), where $A_{2,GS}$ and Ψ_{GS} are the good-solvent values.

z		$A_2(z)$	r
$z^{(1)}$	= 0.056215	0.9926(10)	0.18
$z^{(1.5)}$	= 0.097563	1.5	0.27
$z^{(2)}$	= 0.148726	1.9782(18)	0.36
$z^{(2.5)}$	= 0.225292	2.5	0.45
$z^{(3)}$	= 0.321650	2.9621(27)	0.54
$z^{(3.5)}$	= 0.493088	3.5	0.64
$z^{(4)}$	= 0.728877	3.9433(34)	0.72
$z^{(4.5)}$	= 1.32527	4.5	0.82
$z^{(5)}$	= 2.50828	4.9147(36)	0.89

result $g^*(\rho; z)$ is obtained by performing an extrapolation of the form

$$g(\rho; L, z) = g^*(\rho; z) + \frac{a(\rho; z)}{\sqrt{L}} + O(L^{-1} \ln L). \quad (8)$$

At finite density we should take the limit $L \to \infty$, keeping the polymer volume fraction Φ fixed. In practice we keep the dimensionless combination $\Phi = 4\pi c[\hat{R}_g(L_i, w_i)]^3/3$ fixed, where $\hat{R}_g(L, w)$ is the zero-density radius of gyration (here and in the following we indicate any zero-density quantity with a hat).

In order to determine the crossover behavior, we have performed simulations at the five values $z^{(i)}$, $i = 1, \ldots 5$, considered in Ref. 15, see Table I. They belong to the crossover region between ideal and good-solvent behavior and are such that $A_2(z^{(n)}) \approx n$ (remember that $A_2(z)$ varies between 0 and 5.50). Some additional simulations have also been performed at four values of z such that $A_2(z) = 1.5$, ..., 4.5, where $A_2(z)$ is given in Eq. (4). The explicit values are reported in Table I.

In principle, the crossover functions can also be computed in other models that interpolate between good-solvent and θ behavior. A typical example, which has been widely discussed in the literature, see, e.g., Refs. 11,41,42, is the SAW model with nearest-neighbor interactions (often called interacting SAW model). Another model, quite interesting from a computational point of view, is the extension of the DJ model discussed in Ref. 13, in which an additional energy term associated with triple intersections is considered. Unlike the DJ model, in these models there is a nonvanishing three-body effective coupling, which implies, for instance, that the third virial combination A_3 is positive at the Boyle temperature where $A_2 = 0$. If we take these marginally irrelevant three-body terms into account, the scaling behavior (2) becomes[4,5,13]

$$\mathcal{O}(T, L, c) = \alpha_1 O_G(L, c) h_{\mathcal{O}}(z, u_3, \Phi), \quad (9)$$

where u_3, which parametrizes the effective three-body interaction, vanishes as $1/\ln L$ for $L \to \infty$. As long as the thermal crossover region is considered, i.e., we are in the temperature/degree-of-polymerization region such that $z \gg u_3$ and L is large, we can neglect u_3 in Eq. (9) and reobtain Eq. (2) with $f_{\mathcal{O}}(z, \Phi) = h_{\mathcal{O}}(z, 0, \Phi)$. However, for polymers of finite length, tricritical corrections proportional to u_3 give rise to slowly varying scaling corrections, which make a precise determination of the scaling crossover functions quite difficult. For this reason it is convenient to consider models, like the DJ one, with only two-body repulsion, thereby avoiding unwanted tricritical corrections. Of course, if one wishes to discuss also tricritical effects, the model of Ref. 13 or interacting SAWs should be considered. In this respect, we note that the extended DJ model[13] is computationally much more convenient than the more common interacting SAW model. Indeed, since interactions are soft, one expects the Monte Carlo dynamics to be significantly faster than for interacting SAWs.

III. THE BLOB MODEL

A. The coarse-grained representation of the polymer model

In the multiblob approach one starts from a *coarse-grained representation* (CGR) of the underlying full-monomer (FM) model, which is obtained by mapping a chain of L monomers onto a chain of n blobs, each of them located at the center of mass of a subchain of $m = L/n$ monomers. If the monomer positions are given by $\{\mathbf{r}_1, \ldots, \mathbf{r}_L\}$, one first defines the blob positions $\mathbf{s}_1, \ldots, \mathbf{s}_n$ as the centers of mass of the subchains of length m, i.e.

$$\mathbf{s}_i = \frac{1}{m} \sum_{\alpha=m(i-1)+1}^{mi} \mathbf{r}_\alpha. \quad (10)$$

For the new CG chain $\{\mathbf{s}_1, \ldots, \mathbf{s}_n\}$ one defines several standard quantities. First, one defines its square radius of gyration

$$R^2_{g,b}(n) = \frac{1}{2n^2} \sum_{i,j=1}^{n} (\mathbf{s}_i - \mathbf{s}_j)^2. \quad (11)$$

Such a quantity is always smaller than R^2_g, because of the exact identity

$$R^2_g = R^2_{g,b}(n) + r^2_g(n), \quad (12)$$

where $r_g(n)$ is the average radius of gyration of the blobs. The ratios $R^2_{g,b}(n)/R^2_g$ and $r^2_g(n)/R^2_g$ of their averages over the polymer configurations (we use the same symbol both for the radius of a single chain and for its average; the correct interpretation should be clear from the

context) show a universal crossover behavior, i.e. independent of the nature of the underlying polymer model as long as L and m are large enough. This crossover can be equivalently parametrized in terms of z or of A_2. Explicit zero-density results are reported in App. A.

To define the CGM we proceed as in our previous work,[29,30] defining at first a tetramer model with $n = 4$ blobs. Higher-resolution models with $n > 4$ will be discussed in Sec. V. To determine the four-blob CGM, we compute several intramolecular CGR structural distributions for an isolated chain (zero-density limit). First, we determine the bond-length distributions of the CGR FM model:

$$P_{ij}(r) = \langle \delta(|\mathbf{s}_i - \mathbf{s}_j| - r) \rangle. \tag{13}$$

In the crossover limit at fixed z, the adimensional combination $\hat{R}_g P_{ij}(r)$ converges to a universal crossover function $f^*_{ij}(\rho; z)$, $\rho = r/\hat{R}_g$, which can be computed in the DJ model as described in Sec. II. Second, we will need the distributions of the two equivalent bending angles β_i, of the torsion angle θ, and of the angle β_{13}, defined in the CGR of the polymer model. They are defined as follows:

$$\cos\beta_i = -\frac{\mathbf{b}_i \cdot \mathbf{b}_{i+1}}{|\mathbf{b}_i||\mathbf{b}_{i+1}|}, \tag{14}$$

$$\cos\beta_{13} = \frac{\mathbf{b}_1 \cdot \mathbf{b}_3}{|\mathbf{b}_1||\mathbf{b}_3|}, \tag{15}$$

$$\cos\theta = \frac{(\mathbf{b}_1 \times \mathbf{b}_2) \cdot (\mathbf{b}_2 \times \mathbf{b}_3)}{|\mathbf{b}_1 \times \mathbf{b}_2||\mathbf{b}_2 \times \mathbf{b}_3|}, \tag{16}$$

with $\mathbf{b}_i = \mathbf{s}_{i+1} - \mathbf{s}_i$. In the crossover limit they converge to the TPM distributions $f^*_b(\cos\beta; z)$, $f^*_{b,13}(\cos\beta_{13}; z)$, and $f^*_t(\theta; z)$.

Finally, to determine the intermolecular CGM interactions we will make use of the center-of-mass intermolecular distribution function. It is defined by

$$g_{CM}(r) = \langle e^{-\beta U_{12}} \rangle_{0,\mathbf{r}}, \tag{17}$$

where $\langle\cdot\rangle_{0,\mathbf{r}}$ indicates the average over two isolated polymers, the centers of mass of which are in the origin and in $\mathbf{r}$, respectively, and U_{12} is the intermolecular energy. In the crossover limit $L \to \infty$ at fixed z, $g_{CM}(r)$ converges to a universal function $g^*_{CM}(\rho; z)$.

B. The coarse-grained blob model

The CGM consists of polyatomic molecules of n atoms located in $\{\mathbf{t}_1, \ldots, \mathbf{t}_n\}$. All length scales are expressed in terms of the zero-density radius of gyration, hence all potentials and distribution functions depend on the adimensional combinations $\boldsymbol{\rho} = \mathbf{t}/\hat{R}_g$. In order to have an exact mapping of the CGR of the polymeric system onto the n-blob CGM, one should consider an n-body intramolecular potential, which, for $n > 2$, can be expressed in terms of $3(n-2)$ scalar combinations of the positions of the blobs because of rotational and translational invariance. Even for n as small as 4, this requires considering a function of 6 independent variables. Moreover, since we are computing the potentials in the crossover region, we should additionally consider them as a function of the crossover variable z. Of course, this is far too complex in practice. Hence, we have used two different simplifications.[29,30] First, we use a limited set of interactions. The intramolecular interactions have been modeled by introducing seven different potentials, each of them depending on a single scalar variable. This choice is arbitrary, but, as we have already verified in the good-solvent case,[29,30] it is particularly convenient and works quite well. Second, we have computed the potentials only for five different values of z, $z^{(1)}$, ..., $z^{(5)}$, reported explicitly in Table I. For other values of z we use a simple interpolation, which, as we shall discuss, works quite precisely.

TABLE II: Estimates of $\hat{R}^2_{g,b}/\hat{R}^2_g$ and of A_2 obtained by using the tetramer (t) CGM and the full-monomer (FM) model. The values of z are reported in Table I.

	$\hat{R}^2_{g,b}/\hat{R}^2_g$		$A_2 = B_2/\hat{R}^3_g$	
z	FM	t	FM	t
$z^{(1)}$	0.7553(7)	0.7574(3)	0.9926(10)	0.9763(1)
$z^{(2)}$	0.761(1)	0.7587(5)	1.9782(18)	1.9459(3)
$z^{(3)}$	0.7686(15)	0.7719(5)	2.9621(27)	2.9364(5)
$z^{(4)}$	0.777(2)	0.7844(4)	3.9433(34)	3.9999(7)
$z^{(5)}$	0.787(2)	0.7885(4)	4.9147(36)	4.9105(8)

As in Refs. 29,30, we consider a set of bonding pair potentials: blobs i and j of the tetramer interact with a pair potential $V_{ij}(\rho; z)$ with $\rho = |\mathbf{t}_i - \mathbf{t}_j|/\hat{R}_g$. Because of symmetry we have $V_{13}(\rho; z) = V_{24}(\rho; z)$ and $V_{12}(\rho; z) = V_{34}(\rho; z)$, so that there are only four independent potentials to be determined. Then, we consider a bending-angle potential $V_b(\cos\beta; z)$, a potential $V_{b,13}(\cos\beta_{13}; z)$ and a torsion-angle potential $V_t(\theta; z)$, where β, β_{13}, and θ are defined as in Sec. III A.

To determine the CGM intramolecular potentials, we require the CGM to reproduce the adimensional TPM bond distributions $f^*_{ij}(r; z)$ and the TPM angle distributions defined in Sec. III A. To obtain these distributions, we perform simulations of the DJ model with chains of lengths $L = 1000, 2500$, and 5000 monomers, using the pivot algorithm.[43–48] Then, we extrapolate the relevant quantities by using Eqs. (7) and (8). Once the TPM distributions are known, the potentials are obtained by applying the Iterative Boltzmann Inversion (IBI) scheme.[22,23,49]

The method works quite precisely: The CGM reproduces quite well the target distribution functions. For instance, in Fig. 2 we report the intramolecular distribution function $g_{\rm intra}(\rho)$ computed by using the CGR of the polymer model and the tetramer model for the five values of z we consider. The agreement is excellent. Excellent

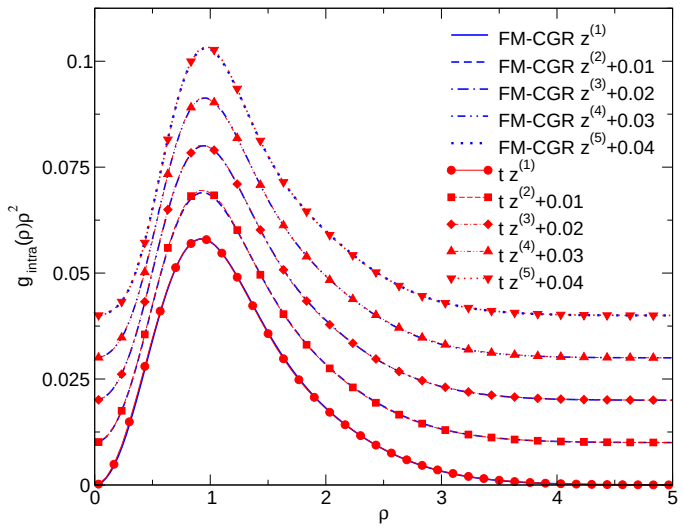

FIG. 2: Intramolecular distribution function $\rho^2 g_{\rm intra}(\rho;z)$. We report tetramer (t) and full-monomer (FM) results at zero density for the values of z reported in Table I. For sake of clarity, results at different values of z are shifted upward according to the legend.

agreement is also observed for the angle distributions (see supplementary material[36]). As a second check of the accuracy of the inversion procedure, we compute the ratio $\hat{R}_{gb}/\hat{R}_g$ both in the polymer model and in the CGM. Again, the results reported in Table II show an excellent agreement.

The potentials are shown in Figs. 3 and 4. Explicit parametrizations are reported in the supplementary material.[36] The bonding pair potentials $V_{12}(\rho;z)$ and $V_{23}(\rho;z)$ change significantly with z. First, the position $\rho_{\rm min}$ of the minimum of the potentials decreases from the good-solvent value[29] $\rho_{\rm min}=0.5$ to 0.3 for $z=z^{(3)}$ and is approximately zero for $z^{(1)}$. This is consistent with what one finds[50] for the random-walk case ($z=0$), for which the bonding pair potential is a parabola, hence $\rho_{\rm min}=0$. Second, the potential becomes softer at the origin as z decreases. For instance, $\Delta_{12}(z)=\beta[V_{12}(0;z)-V_{12}(\rho_{\rm min};z)]$ decreases from the good-solvent value 0.8 to 0 as z decreases. More precisely, $\Delta_{12}(z)\approx 0, 0.4, 0.7$ for $z=z^{(1)},z^{(3)},z^{(5)}$, respectively. As before, this is due to the fact that excluded-volume effects become less relevant as z decreases. Potential $V_{13}(\rho;z)$ shows qualitatively the same behavior as a function of z. Potential $V_{14}(\rho;z)$ has an approximate Gaussian shape for all values of z. As expected $V_{14}(0;z)$ decreases significantly with decreasing z. Since excluded-volume effects decrease in this limit, overlaps are less penalized.

In Fig. 4 we report the angular potentials. The bending potential changes significantly with z. For large z folded configurations with $\cos\beta\approx 1$ are penalized, while for small z, they are slightly favored. The torsion potential becomes very small for small values of z: the tetramer becomes more flexible as the excluded-volume interactions become less effective. For instance $\beta[V_t(\pi;z^{(1)})-V_t(0;z^{(1)}]\approx 0.01$. The four-body bending potential $V_{b,13}(\cos\beta_{13};z)$ changes only in the region in which $\cos\beta_{13}>0$. In particular, by increasing z, $\Delta_{b,13}=\beta[V_{b,13}(1;z)-V_{b,13}(0;z)]$ decreases, signalling that more elongated conformations are preferred as excluded-volume effects increase.

As for the intermolecular potentials, we have made again some drastic simplifications. First, in the spirit of the multiblob approach, we neglect interactions among three or more tetramers. The potential between two tetramers is still a function of the $6(n-1)$ relative positions of the blobs, which is again far too complex. We have thus simplified the model by considering a single intermolecular central pair potential $W(\rho;z)$: all blobs interact with the same potential, irrespective of their positions along the tetramer. As shown in Refs. 29,30 this drastic simplification works quite well. Such a potential has been obtained by requiring the CGM to reproduce the TPM center-of-mass intermolecular distribution function $g^*_{CM}(\rho;z)$. The potential $W(\rho;z)$ has been parametrized as

$$\beta W(\rho;z)=c_1(z)\exp(-c_2(z)\rho^2), \qquad (18)$$

in terms of two unknown z-dependent parameters $c_1(z)$ and $c_2(z)$. They have been determined following the approach of Ref. 51. Parametrization (18) looks adequate. The CGM reproduces quite precisely the FM result, see Fig. 5. As a check of the accuracy of the procedure, we also compare the second-virial combination A_2. Again, the results reported in Table II show good agreement (differences are less than 2%). The intermolecular potential is shown in Fig. 4. As expected, in the crossover region from good-solvent to θ behavior one observes a decrease of its strength and a slight decrease of its spatial range.

The results reported above give the tetramer potentials for five different values of z, each of which corresponds to a different value $A_2^{(n)}$ of the second-virial combination A_2, see Table I. To define the model for all values of z we use a simple linear interpolation formula. Given z, we first determine $A_2(z)$ by using Eq. (4) and then an integer $1\le n_1\le 5$ such that $A_2^{(n_1)}\le A_2(z)\le A_2^{(n_1+1)}$ ($n=6$ corresponds to the good-solvent case, hence $A_2^{(6)}=5.500$). Then, for each potential we set (σ may be ρ or an angular variable)

$$V(\sigma;z) = \frac{A_2(z)-A_2^{(n_1)}}{A_2^{(n_1+1)}-A_2^{(n_1)}}V(\sigma;z^{(n_1+1)}) - \frac{A_2(z)-A_2^{(n_1+1)}}{A_2^{(n_1+1)}-A_2^{(n_1)}}V(\sigma;z^{(n_1)}). \qquad (19)$$

As a check of the accuracy of this interpolation we have chosen four values of z such that $A_2=1.5$, 2.5, 3.5, 4.5, see Table I. For these values we have computed the

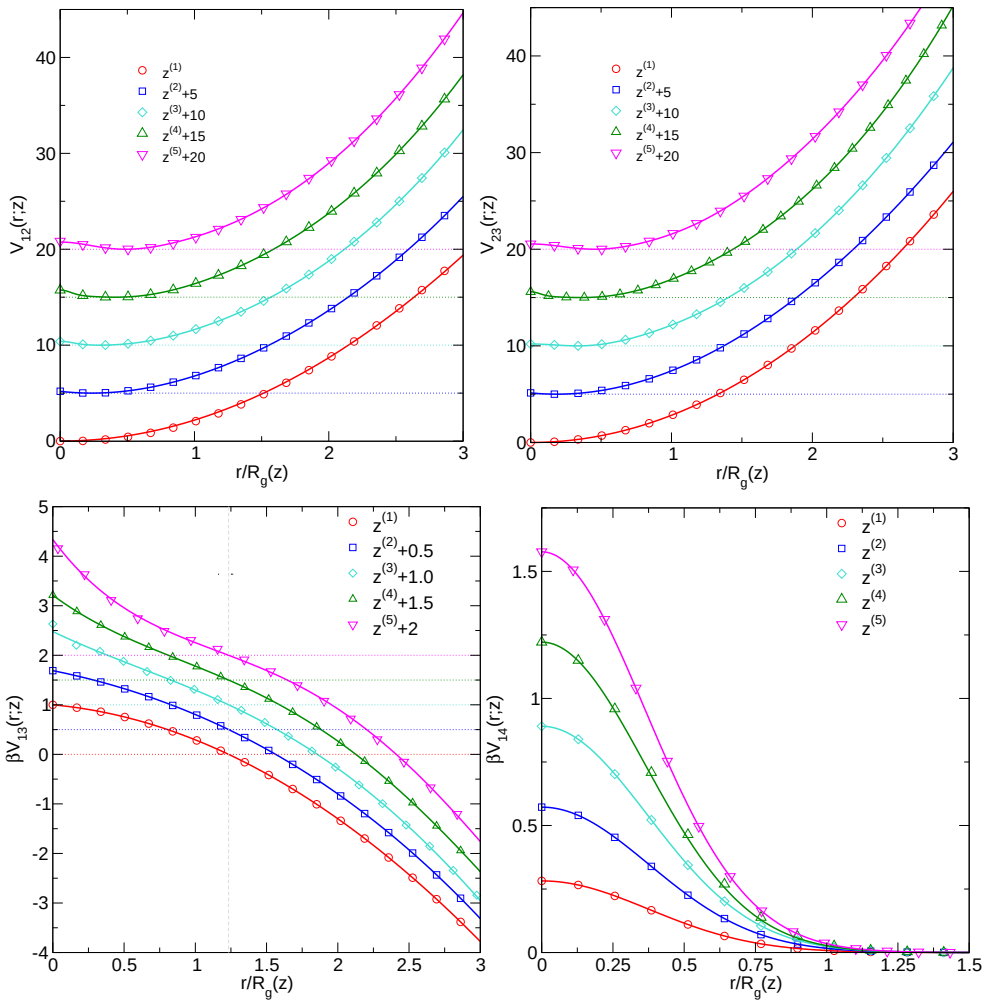

FIG. 3: Intramolecular tetramer bond potentials for five values of z reported in Table I: points correspond to the numerical estimates, while the solid lines are the interpolations reported in the supplementary material.[36] For the sake of clarity, results at different values of z are shifted upward according to the legend.

tetramer potentials using the interpolation formula (19). Then, we have computed again A_2 for each value of z by using the tetramer CGM. Results are consistent—differences are at most 1%—confirming the accuracy of the interpolation we use (see supplementary material[36] for more details).

IV. COMPARING TETRAMER AND FULL-MONOMER PREDICTIONS

In this section, we compare the CGM structural predictions with those obtained for the CGR of the polymer model. In Sec. IV A we extend the discussion of Sec. III B at zero density, while in Sec. IV C we consider the semidilute regime. Here we compare the CGM results with the results of FM simulations at finite density, discussed in Sec. IV B. Beside considering the tetramer model, we shall also discuss the simpler single-blob (SB) model, in which each polymer is represented by a monoatomic molecule located in the polymer center of mass. The SB potentials in the θ-to-good-solvent crossover regime were computed in Refs. 14,41,42 using the self-avoiding walk model. Here we perform the same computation more carefully, by using the DJ model. An explicit parametrization that satisfies all theoretical constraints and reproduces the good-solvent results of Ref. 14 is reported in the supplementary material.[36]

A. Zero-density results

By construction, the tetramer CGM reproduces all CGR bond-length distributions. However, it is far from obvious that the distributions of other structural intramolecular quantities are correctly reproduced. In Fig. 6 we report the distribution of the ratio $R = \hat{R}_{g,b}/\langle \hat{R}_g^2 \rangle^{1/2}$, where $\hat{R}_{g,b}$ is the radius associated with

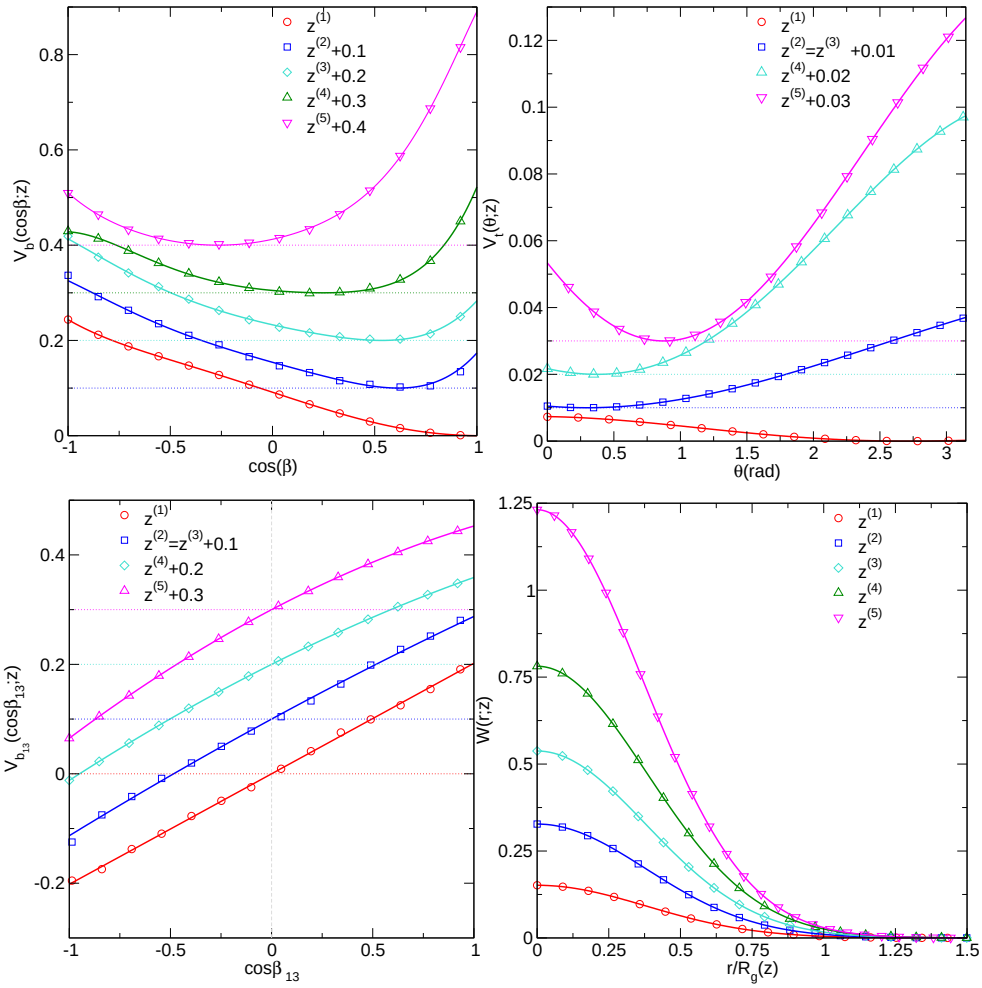

FIG. 4: Tetramer angular and intermolecular potentials for five values of z reported in Table I: points correspond to the numerical estimates, while the solid lines are the interpolations reported in the supplementary material.[36] For the sake of clarity, results at different values of z are shifted upward according to the legend.

a single chain, while $\langle \hat{R}_g^2 \rangle$ is the average squared radius of gyration. The agreement is excellent for all values of z we consider. This is a nontrivial check of the quality of the multiblob representation since this distribution is not directly related to the bond-length distributions nor to those of the intramolecular angles we consider. Clearly, the tetramer CGM correctly models shape and size of the polymer in the whole crossover region.

It is also of interest to compare the predictions for the virial coefficients defined in Eq. (1). Since we matched the pair distribution function $g_{CM}(r)$, the combination $A_2 = B_2 \hat{R}_g^{-3}$ should be the same in the CGM and in the polymer model, as we have already verified in Sec. III B. Here we compare the third-virial combination $A_3 = B_3 \hat{R}_g^{-6}$. Differences between the CGM and the polymer results allow us to quantify the importance of the three-polymer interactions that are not fully taken into account by the CGM. Beside tetramer and FM results, we also report estimates obtained by using the SB model. The results are reported in Table III. The SB results underestimate quite significantly the FM results: the relative deviations increase from 19% for $z = z^{(5)}$ to 30% for $z = z^{(1)}$. The tetramer results are significantly better. Close to the good-solvent regime ($z \gtrsim z^{(4)}$) deviations are approximately 3%. As z is lowered, differences increase: for $z = z^{(1)}$, we find a 9% difference. It is important to note that, although in all cases the observed differences for A_3 increase as the θ point is approached, this does not imply that the difference between the CGM and FM pressure increases when lowering z. Indeed, perturbation theory gives $A_n/A_2 \approx z^{n-1}$ for $z \to 0$. Therefore, the third and higher-order virial contributions to the pressure become increasingly less relevant as z decreases. As a consequence, as we discuss in Sec. IV C, the CGM provides increasingly more accurate estimates of the pressure as the θ point is approached.

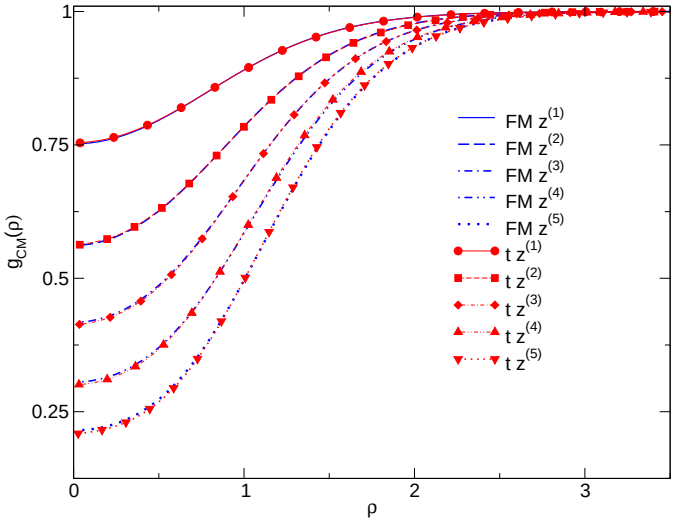

FIG. 5: Radial distribution functions for a pair of isolated chains as a function of the center-of-mass separation $\rho = r/\hat{R}_g$. We report tetramer (t) and full-monomer (FM) results at zero density for five values of z reported in Table I.

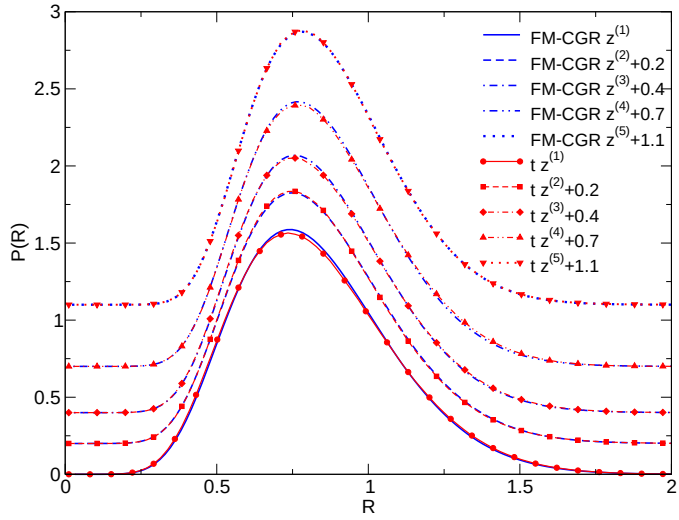

FIG. 6: Distribution of the ratio $R = R_{g,b}/\sqrt{\langle \hat{R}_g^2 \rangle}$. We report tetramer (t) and full-monomer (FM) results at zero density for the values of z reported in Table I. For the sake of clarity, results at different values of z are shifted upward according to the legend.

B. Intermezzo: finite-density thermodynamics by full-monomer simulations

In order to discuss the behavior of the CGM in the semidilute regime, we need to obtain FM reference data. For this reason we have performed an extensive study of the DJ model at finite density. For the five values of z, $z^{(1)}$, ..., $z^{(5)}$, reported in Table I we have performed

TABLE III: Estimates of A_3 for the full-monomer (FM) model, for the tetramer (t), and single-blob (SB) CGMs. We consider values $z^{(n)}$ defined in Table I. The full-monomer (FM) results for $z^{(1)}$, $z^{(2)}$, $z^{(3)}$, $z^{(4)}$, and $z^{(5)}$, are the direct MC estimates of Ref. 15; in the other cases we use the interpolation formula $A_3(z)$ reported in Table III of Ref. 15.

z	FM	t	SB
$z^{(1)}$	0.0849(8)	0.077(1)	0.059
$z^{(1.5)}$	0.276	0.261(6)	0.197
$z^{(2)}$	0.6061(30)	0.553(8)	0.442
$z^{(2.5)}$	1.15	1.10(2)	0.867
$z^{(3)}$	1.843(8)	1.74(2)	1.404
$z^{(3.5)}$	2.89	2.85(3)	2.264
$z^{(4)}$	4.021(13)	3.95(4)	3.164
$z^{(4.5)}$	5.72	5.67(5)	4.569
$z^{(5)}$	7.243(22)	7.02(6)	5.827

simulations for several values of Φ and several values of L ranging between 100 and 2000. As in our previous work,[52] we use a combination of pivot,[43–47] cut-and-permute,[52–54] and reptation moves. Since the penalty parameter w is quite small, the algorithm is quite efficient and for $z^{(1)}$, ..., $z^{(4)}$ we are able to simulate polymer systems for densities up to $\Phi = 30$. For $z = z^{(5)}$, i.e. close to the good-solvent regime, the largest density considered corresponds to $\Phi = 20$. In the finite-density simulation we should also fix the volume $V = M^3$ of the box. As in Ref. 52 we fix the box size so that the number N of polymers in the box is never smaller than 100 (typically $150 \lesssim N \lesssim 1000$). We measure the relevant CGR intramolecular and intermolecular distribution functions, needed for a detailed comparison with the CGM results. Moreover, to compare the thermodynamics we compute

$$K = \frac{\partial \beta \Pi}{\partial c}, \tag{20}$$

where $c = N/V$. This quantity is determined as in Ref. 52. Using the compressibility rule[55] we can relate K to the total structure factor that can be easily measured in simulations. If we define

$$S(\mathbf{k}) \equiv \frac{1}{L^2 N} \left\langle \left| \sum_{j=1}^{N} \sum_{\alpha=1}^{L} \exp(i\mathbf{k}\cdot\mathbf{r}_\alpha^{(j)}) \right|^2 \right\rangle, \tag{21}$$

then we have

$$\frac{1}{K} = \lim_{k\to 0} S(\mathbf{k}). \tag{22}$$

Since we work in a finite box of volume M^3, we must quantify the finite-volume effects. For fluids they have been extensively discussed, see, e.g., Refs. 56 and references therein. In general, at fixed Φ finite-volume quantities converge to their infinite-volume counterpart (if we consider distribution functions or the structure factor we

should, of course, take the limit at fixed r or k) with corrections of order M^{-3}. We find that these corrections are smaller than or, at most, of the same order as the statistical errors. To give an example, let us discuss in more detail the structure factor $S(\mathbf{k})$. If we assume

$$S(\mathbf{k}; M) = S(\mathbf{k}; \infty) + \frac{\alpha(\mathbf{k})}{M^3} + O(M^{-6}), \qquad (23)$$

then, we have

$$S(\mathbf{k}; M) - S(\mathbf{k}; \infty) = \frac{1}{7}\left[S(\mathbf{k}; M/2) - S(\mathbf{k}; M)\right] + O(M^{-6}). \qquad (24)$$

Hence, a rough estimate of the size effects can be obtained by computing the same quantity for two boxes of linear size M and $M/2$, respectively. To give an idea of the effect, let us consider two cases. In the good-solvent regime, for $\Phi = 10$, $L = 250$, we have performed simulations with $M = 32$ ($N = 100$) and $M = 64$ ($N = 802$). For $k = 2\pi/32$, the smallest momentum which is present in both cases, we obtain $S(\mathbf{k}; M) = 0.01319(4)$ and $0.01316(2)$ for $M = 32, 64$, respectively. Clearly, the systematic error on the estimate obtained by using $M = 64$ (the only one we use) is negligible. In the opposite limit, consider $z = z_1$, $\Phi = 15$, $L = 2000$. For $k = 2\pi/64$, we obtain $S(\mathbf{k}; M) = 0.09831(6)$, $0.09853(8)$ for $M = 64, 128$, respectively. Again, Eq. (24) indicates that finite-volume corrections on the largest-lattice result are significantly smaller than statistical errors. Hence, to obtain the TPM results it is enough to extrapolate the finite-L data at the same value of Φ by using Eqs. (7) or (8).

In the simulation we estimate $S(\mathbf{k})$ for two different wave vectors: $\mathbf{k}_1 = (2\pi/M, 0, 0)$ and $\mathbf{k}_2 = (4\pi/M, 0, 0)$, where M is the linear size of the cubic box. Then, we define[52]

$$K_{\rm est} = \frac{\hat{k}_2^2 - \hat{k}_1^2}{\hat{k}_2^2 S(\mathbf{k}_1) - \hat{k}_1^2 S(\mathbf{k}_2)}, \qquad (25)$$

where $\hat{k} = 2\sin(k/2)$, $k_1 = 2\pi/M$, and $k_2 = 4\pi/M$. As discussed in Ref. 52, the estimator $K_{\rm est}$ of the inverse compressibility converges to K with corrections of order M^{-4}, i.e.

$$K_{\rm est}(L, M) = K(L) + \frac{a(L)}{M^4}, \qquad (26)$$

where we have only included the leading correction. It turns out that this term is not negligible, hence an additional extrapolation is needed to obtain $K(L)$. Of course, $K_{\rm est}$ also depends on Φ and z, but since they do not play any role here—we work at fixed density and z—they are omitted. To go further, we must specify the L dependence of $a(L)$. Since $a(L)$ corresponds dimensionally to a fourth power of a length, we expect on general grounds and verify numerically in a few cases that $a(L) \sim \hat{R}_g^4 \sim L^2$, with corrections that decay as $L^{-1/2}$: $a(L) = L^2(b + cL^{-1/2})$. Since the infinite-volume $K(L)$ should behave as $R(L, z)$ in Eq. (7), we end up with the asymptotic expansion

$$K_{\rm est}(L, M) = K^* + \frac{k}{\sqrt{L}} + \frac{L^2}{M^4}\left(b + \frac{c}{\sqrt{L}}\right), \qquad (27)$$

where $K^* = K^*(z, \Phi)$ is the TPM result. For each Φ and z we have therefore fitted our simulation results to Eq. (27), keeping K^*, k, b, and c as free parameters, in order to obtain the TPM prediction $K^*(z, \Phi)$.

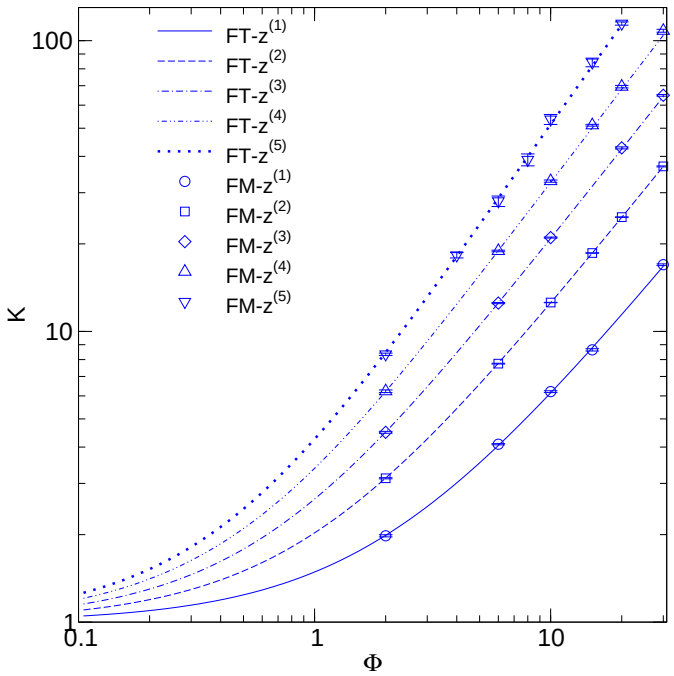

FIG. 7: TPM estimates of K for different values of z, see Table I. We report full-monomer (points, FM) and field-theory (lines, FT) results.

It is interesting to compare the numerical results with the field-theoretical (FT) predictions of Ref. 5 (the relevant formulae are summarized in App. B). In all cases we observe very good agreement, see Fig. 7. For $z = z^{(1)}$, $z^{(2)}$, and $z^{(3)}$, in the quite large range of densities we consider, $\Phi \le 30$, the relative differences are always less than 1%. For the two largest values of z, differences are somewhat larger but remain below 4%. Note that similar conclusions were reached in Ref. 52 for the good-solvent case. Hence, the parametrization of Ref. 5 of the FT results appears to be quite accurate in the whole crossover regime.

For $\Phi \to \infty$ and any finite z, $K(z, \Phi)$ converges[15] to $K_{\rm as}(z, \Phi) \equiv k_{FM}(z)\Phi$ with $k_{FM}(z) = 6\sqrt{\pi} z \alpha_g^{-3}(z)$, where $\alpha_g(z)$ is the swelling factor of the zero-density radius of gyration, computed explicitly in Ref. 15. For $z = z^{(1)}, \ldots, z^{(5)}$ we obtain $k_{FM}(z) = 0.543, 1.27, 2.32, 4.07, 8.40$, respectively. For each value of z, we can compare our result for the largest value of Φ with this asymptotic prediction. For $\Phi = 30$, we ob-

tain from simulation $K(z,\Phi) = 16.73(6)$, 37.1(2), and 64.8(3), to be compared with $K_{\rm as}(z,\Phi) = 16.3$, 38.1, and 69.6, for $z = z^{(1)}$, $z^{(2)}$, and $z^{(3)}$, respectively. Clearly, for such large value of Φ the asymptotic formula holds approximately only for $z \lesssim z^{(2)}$. For larger values of z, the linear behavior sets in for values of Φ that are significantly larger than 30.

Finally, we should mention that Ref. 15 also gave a prediction for $Z(z,\Phi)$ [Eq. (4.24) of Ref. 15] valid for $z \to \infty$ and $\Phi \lesssim \Phi_{\rm max}(z) \sim z^{2.53}$. Requiring an error of at most 5%, the asymptotic expansion was found to be predictive for $z \gtrsim 2$, $\Phi \lesssim (z/2)^{2.53}$. The first condition implies that we can only consider $z = z^{(5)}$, while the second condition implies that Φ should be relatively small, $\Phi \lesssim 2$. In this density range, by using the equation of state reported in the supplementary material,[36] we find that the asymptotic formula reproduces $Z(z^{(5)},\Phi)$ with an error of at most 4%, confirming the correctness of the numerical estimates of Ref. 15.

C. Comparison in the semidilute regime

Let us now compare the CGM predictions with the polymer CGR results at finite density. Let us begin by comparing the intramolecular distribution function. Results for $z = z^{(1)}$ and $z = z^{(3)}$ are reported in Fig. 8. In all cases the agreement is excellent, even for $\Phi = 4$. Similar conclusions are reached for the finite-density distribution of $R_{g,b}$, see Fig. 9. Clearly, the tetramer model correctly reproduces the large-scale structure of the polymer even in the presence of significant polymer-polymer overlap. Note that this is not the case in the good-solvent regime.[29] In that case, for $\Phi \approx 4$ the tetramer is more swollen than the polymer: the probability for two blobs to be at a given distance $\rho \lesssim 1$ is significantly smaller in the tetramer than in the polymer. Analogously, $R_{g,b}$ is typically larger for the tetramer than for the polymer.

Let us now compare the intermolecular structure. In Fig. 10 we report the center-of-mass distribution function $g_{CM}(r)$ for the tetramer, the SB model, and from FM simulations. For $z = z^{(1)}$ both the tetramer and the SB model correctly reproduce the polymer structure, even for $\Phi = 4$. Clearly, many-body interactions are weak, hence do not influence significantly the polymer behavior, even in the presence of significant overlap among the polymers. For $z = z^{(3)}$ the SB model reproduces $g_{CM}(r)$ for $\Phi = 1$, while discrepancies are observed for $\Phi = 4$. On the other hand, the tetramer model is quite accurate, even for $\Phi = 4$. Many-body interactions are relevant, but are reasonably taken into account by the tetramer model.

Let us finally, discuss the thermodynamics, comparing the estimates of $K(z,\Phi)$ for polymers with those obtained by using the SB and the tetramer model, see Fig. 11 (see supplementary material[36] for tables of data). For $z = z^{(1)}$ tetramer results are on top of the FM results, even for $\Phi = 10$: at this density we obtain $K = 5.96(4)$ (tetramer), $K = 6.15(3)$ (FM). For $z = z^{(2)}$ discrepancies are small (the relative difference is 5% for $\Phi = 6$ and 8% for $\Phi = 10$) and so are they for $z = z^{(3)}$ (9% for $\Phi = 10$). For $z = z^{(4)}$ and $z^{(5)}$ we observe larger differences, the relative difference being larger than 10% for $\Phi \gtrsim 5$ and 3, respectively. Thermodynamic results are completely consistent with the structural ones.

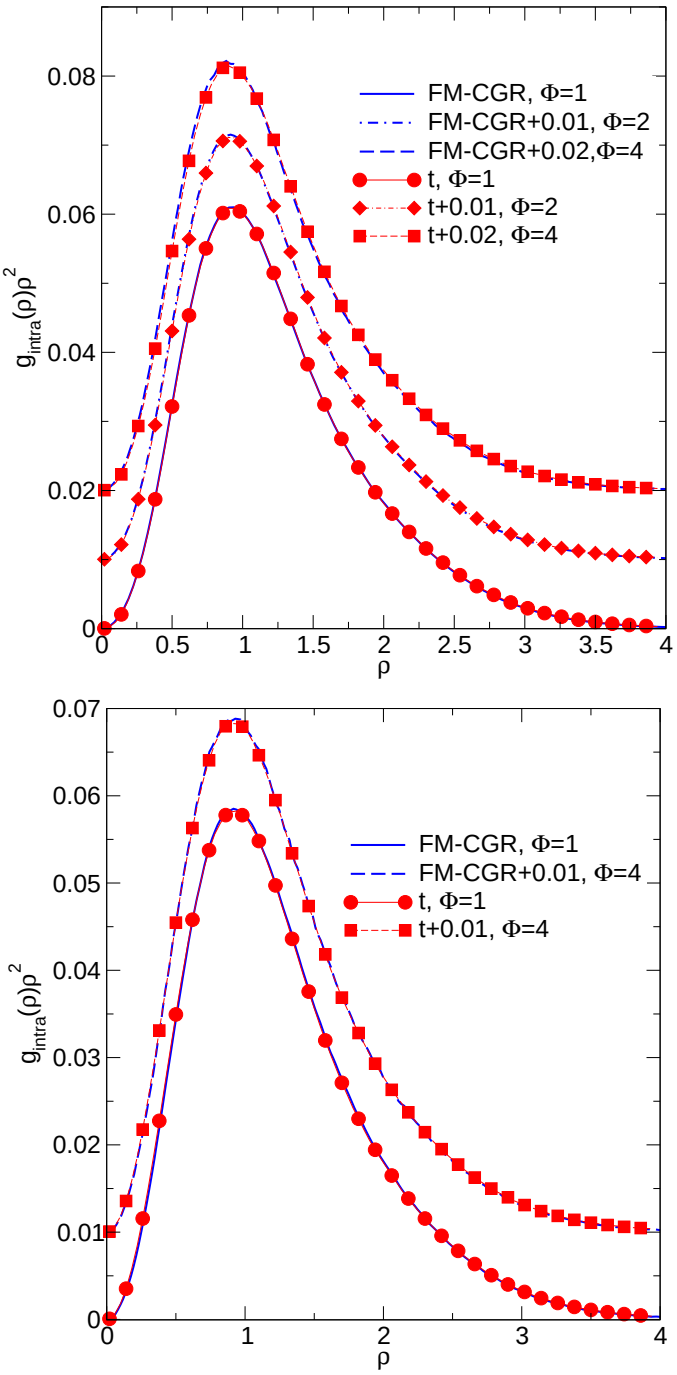

FIG. 8: Intramolecular distribution function as a function of $\rho = r/\hat{R}_g$, for $z = z^{(3)}$ (top) and $z = z^{(1)}$ (bottom). We report full-monomer (FM-CGR) and tetramer (t) results.

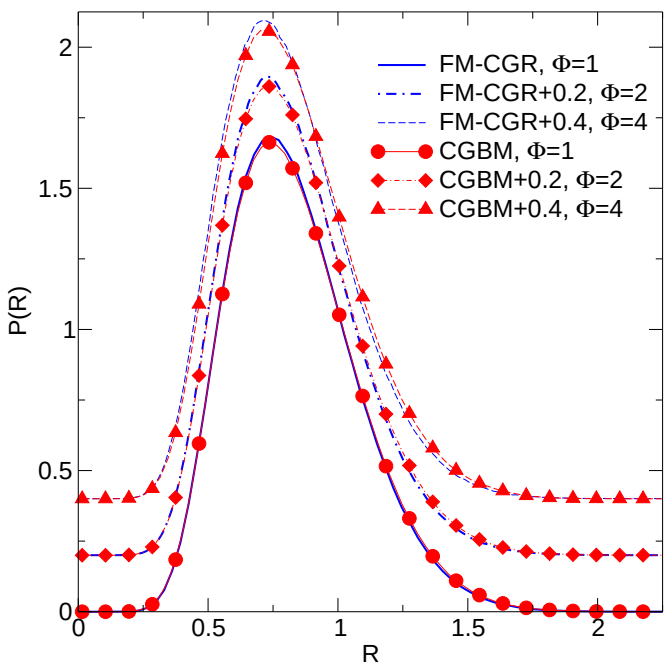

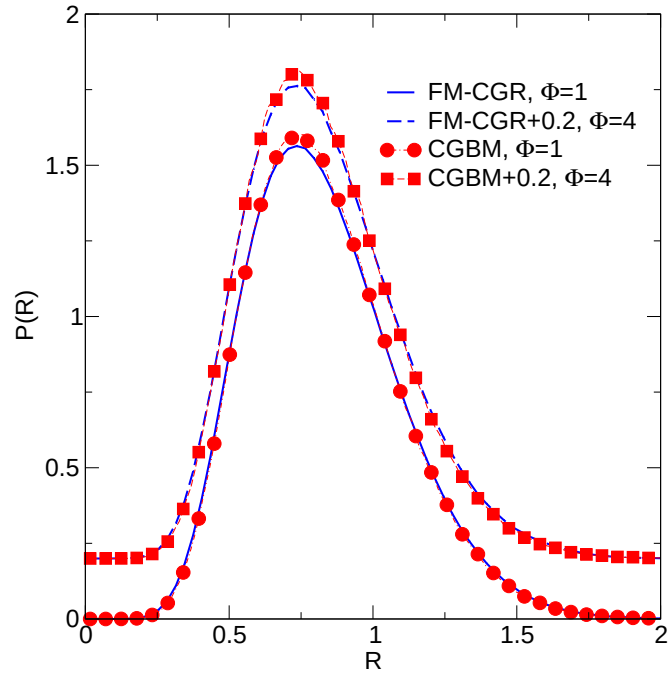

FIG. 9: Distribution of $R = R_{g,b}(\Phi)/\langle \hat{R}_g \rangle$ for $z = z^{(3)}$ (top) and $z = z^{(1)}$ (bottom). We report full-monomer (FM-CGR) and tetramer (t) results.

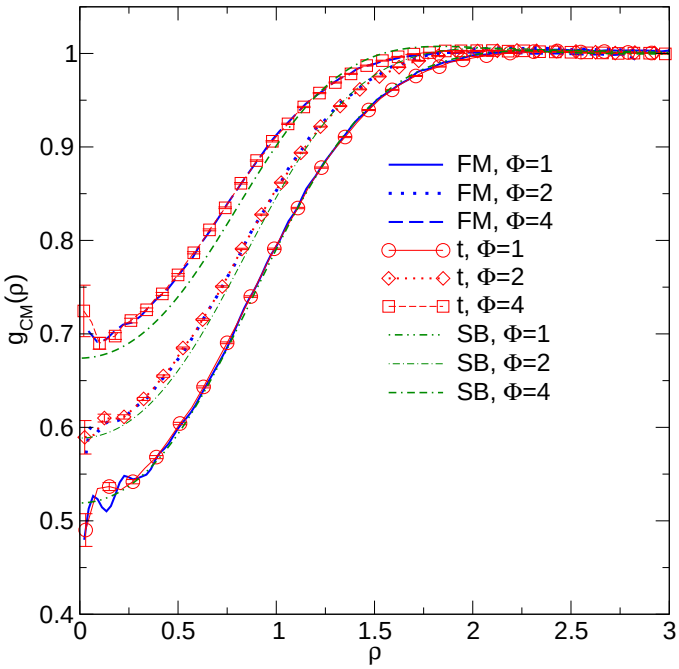

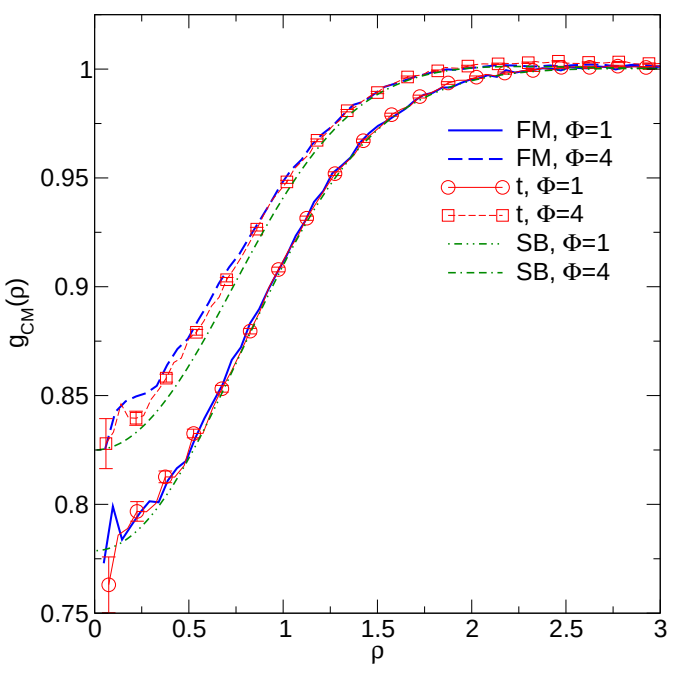

FIG. 10: Intermolecular center-of-mass pair distribution function as a function of $\rho = r/\hat{R}_g$, for $z = z^{(3)}$ (top) and $z = z^{(1)}$ (bottom). We report full-monomer (FM), single-blob (SB) and tetramer (t) results.

For $z \lesssim z^{(3)}$, i.e. for systems such that $A_2 \lesssim 3$ (i.e., $A_2/A_{2,GS} \lesssim 0.55$, where $A_{2,GS} = 5.50$ is the good-solvent value), the tetramer model reasonably works also deep in the semidilute regime. On the other hand, for larger values of z, many-blob interactions begin to play a role. Hence, in this region, the model is only predictive for Φ not too large, i.e. for densities such that blob-blob overlaps are rare.

It is also interesting to compare the thermodynamic predictions for the SB model. For $z = z^{(1)}$ and $z = z^{(2)}$ the SB model gives estimates of K that are close to the tetramer and FM ones. Differences are observed

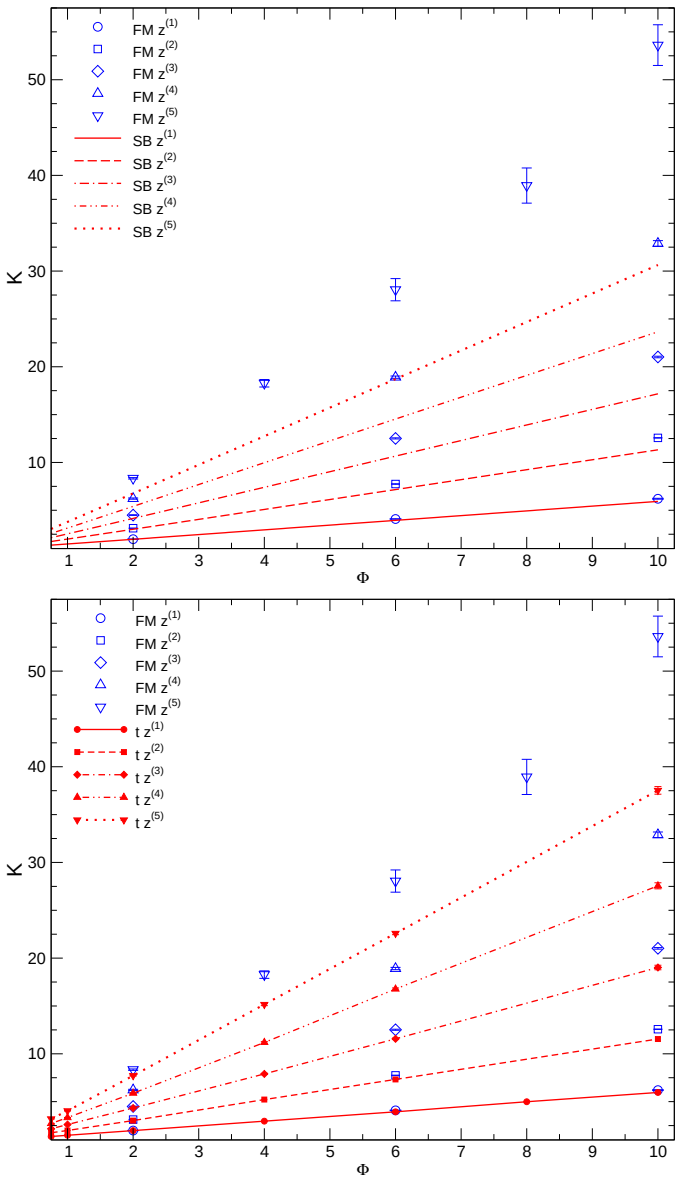

FIG. 11: Inverse compressibility K as predicted by full-monomer (FM) simulations, the single-blob (SB) model (top), and the tetramer (t) model (bottom).

for $z \gtrsim z^{(3)}$: in this regime the SB model significantly underestimates K as long as $\Phi \gtrsim 1$.

D. Comparison for $\Phi \to \infty$ and random-phase approximation

We wish now to compare the thermodynamic behavior for large values of Φ. For the polymer system, we have $K(z,\Phi) \approx K_{\rm as}(z,\Phi) = k_{FM}(z)\Phi$, where $k_{FM}(z)$ is reported in Sec. IV B. We now compute the large-Φ behavior of $K(z,\Phi)$ for the CG models, using the fact that the random-phase approximation (RPA)[55] is exact at large density for systems with soft potentials. For the SB model, we start from the virial pressure

$$Z_{SB}(z;\Phi) = 1 - \frac{\Phi}{2}\int_0^\infty \frac{\partial \beta V_{SB}(\rho;z)}{\partial\rho} g_{CM}(\rho;z,\Phi)\,\rho^3 d\rho. \tag{28}$$

In the RPA, we set $g_{CM}(r;z,\Phi) = 1$, a property which is rigorously true for $\Phi \to \infty$. Integrating by parts we end up with the usual RPA expression[55]

$$Z_{SB}(z,\Phi) = 1 + \frac{1}{2}\Phi k_{SB}(z)$$
$$k_{SB}(z) = 3\int_0^\infty \beta V_{SB}(\rho;z)\,\rho^2 d\rho, \tag{29}$$

from which we obtain $K_{SB}(z,\Phi) = 1 + \Phi k_{SB}(z)$. The function $k_{SB}(z)$ is reported in the supplementary material[36] and in Table IV for some specific values of z. The RPA expression (29) reproduces the SB compressibility factor at the 1% level for $z = z^{(1)}$ for all values of Φ. For larger values of z it provides a very good approximation for $\Phi \gtrsim 3$ (deviations are at most 2% for $\Phi = 3$ and are less than 1% for $\Phi \geq 8$). For smaller densities deviations are larger, due to the fact that the small-density behavior is not correctly reproduced (compare $k_{SB}(z)$ with the estimates of A_2 reported in Table I).

The RPA expression (29) can be extended to the tetramer model. Starting from the expression of the pressure in terms of the atomic virial and assuming the absence of blob-blob correlations among blobs belonging to different tetramers, we obtain for a CGM with n blobs (see also Ref. 57)

$$Z(z,\Phi) = 1 + \frac{1}{2}\Phi k_n(z) \qquad k_n(z) = 3n^2\int_0^\infty \beta W(\rho;z)\,\rho^2 d\rho. \tag{30}$$

where $W(\rho;z)$ is the intermolecular potential. Estimates of $k_4(z)$ are reported in Table IV. In the good-solvent case, using the transferability assumption, the integral should scale as $n^{-3\nu}$, so that we obtain $k_n(z=\infty) = 3.204 n^{2-3\nu}$ (the prefactor has been fixed by using the explicit rescaling factor reported in Ref. 30).

Knowledge of the constants $k(z)$ allows us to compute the deviations between CGM and FM results for $\Phi \to \infty$

TABLE IV: Large-Φ coefficients $k_{SB}(z)$, $k_4(z)$, and $k_{FM}(z)$ for five intermediate values of z, see Table I, and for the good-solvent case ($z = \infty$). For $n \geq 4$, $k_n(z=\infty) = 3.204 n^{2-3\nu}$.

z	$k_{SB}(z)$	$k_4(z)$	$k_{FM}(z)$
$z^{(1)}$	0.4956	0.501	0.543
$z^{(2)}$	1.0352	1.083	1.270
$z^{(3)}$	1.6271	1.778	2.320
$z^{(4)}$	2.2750	2.643	4.072
$z^{(5)}$	2.9731	3.643	8.504
∞	3.4163	4.584	—

without the need of simulations, since

$$\frac{K_n(z,\Phi)}{K_{FM}(z,\Phi)} \approx \frac{k_n(z)}{k_{FM}(z)} \tag{31}$$

for $\Phi \to \infty$. For $z = z^{(1)}$, $k_{SB}(z)$ and $k_4(z)$ are close to $k_{FM}(z)$: the SB $K(z,\Phi)$ (or equivalently $Z(z,\Phi)$) differs from the corresponding polymer quantity by 9% for large Φ. For such a small value of z, there is little advantage in using the tetramer model if one is only interested in the thermodynamics: the difference decreases only to 8%. For $z = z^{(2)}$ differences are larger: 18% and 15% for the SB and tetramer model, respectively. For larger values of z, instead, it is quite clear that both the SB and the tetramer model grossly underestimate the correct polymer pressure deep in the semidilute regime.

V. TRANSFERABILITY IN THE NUMBER OF BLOBS

A. Transferability: general considerations

In the previous section we have determined a CG tetramer model appropriate to describe the θ-to-good-solvent crossover. It was found that the predictions of the tetramer model are accurate up to a value of the density $\tilde{\Phi}(z)$, which increases when z decreases towards the θ region. Above $\tilde{\Phi}(z)$ the tetramer model is observed to deviate from the FM results and to approach the RPA predictions at large Φ. We wish now to extend the CG model to a larger number n of blobs per chain, which is the key ingredient to increase $\tilde{\Phi}$. In the good-solvent case, the basic transferability assumption is that the tetramer potentials, expressed in terms of the blob radius of gyration $\hat{r}_g$, provide an accurate CGM for any number of blobs. For $z = \infty$, the approach is therefore the following. First, we express any tetramer bonding potential $V_{ij}(\rho; n = 4)$, $\rho = r/\hat{R}_g$, in terms of $\sigma = r/\hat{r}_g$:

$$\hat{V}_{ij}(\sigma; n = 4) = V_{ij}(\sigma \mathcal{R}_4), \tag{32}$$

where $\mathcal{R}_4 = \hat{r}_g/\hat{R}_g$ for the tetramer. Then, the potentials for the n-blob model are defined by

$$\begin{aligned}
&\hat{V}_{12}(\sigma; n) = \hat{V}_{n-1,n}(\sigma; n) = \hat{V}_{12}(\sigma; 4), \\
&\hat{V}_{ij}(\sigma; n) = \hat{V}_{23}(\sigma; 4) \qquad |i-j| = 1, i \neq 1, n-1, \\
&\hat{V}_{ij}(\sigma; n) = \hat{V}_{13}(\sigma; 4) \qquad |i-j| = 2, \\
&\hat{V}_{ij}(\sigma; n) = \hat{V}_{14}(\sigma; 4) \qquad |i-j| \geq 3.
\end{aligned} \tag{33}$$

Note, that blobs i and j with $|i-j| > 3$ always interact with potential $\hat{V}_{14}(\sigma; 4)$ to guarantee the local self-repulsion, which is necessary to obtain a good-solvent CGM. The angular potentials are instead unchanged when increasing the number of blobs per chain. If $\hat{R}_g$ is used as reference length scale, i.e. we consider $V_{ij}(\rho; n)$ with $\rho = r/\hat{R}_g$, these relations imply the rescalings $V(\rho; n) = V(\rho \mathcal{R}_4/\mathcal{R}_n; 4)$.[30]

To justify the previous relations, we should first note the dual interpretation of the coarse-graining procedure. Up to now, we have considered two blob models with n_1 and n_2 blobs each as providing two different representations (with different resolutions) of the same polymer chain. However, since polymer chains are fractals, hence scale invariant, for large degree of polymerization L, the multiblob model can be given a different interpretation. We assume now that the number m of monomers belonging to a blob is fixed, so that CGMs with n_1 and n_2 blobs are CGRs with the *same* resolution of polymer chains of different lengths, $L_1 = n_1 m$ and $L_2 = n_2 m$, respectively. Within this dual interpretation it is easy to justify transferability. First, we note that, to a very good approximation, the size of the blob depends only on m and not on the length of the chain. The latter nontrivial property was verified for $n \geq 4$ in App. A of Ref. 29. Indeed, since $\hat{R}_g \sim L^\nu$ and $\hat{r}_g/\hat{R}_g \sim n^{-\nu}$ with good precision for $n \geq 4$, we have $\hat{r}_g \sim m^\nu$, which depends only on m and not on L. Therefore, $\hat{r}_g$ is the same for the two CGMs. Second, we assume that the interactions have little dependence on the chemical distance between the blobs, except for the case in which the blobs are very close along the chain, and are insensitive to the length of the CGM. If this holds, potentials are the same for the two CGMs, i.e. they can be *transferred* from one model to the other one. If we wish to use this result within the original CG interpretation, we should simply note that potentials are invariant, if $\hat{r}_g$ is the basic length scale. If $\hat{R}_g$ is used instead, a rescaling of the length scale should be performed.

Let us now consider the case of polymer chains in the thermal crossover region. Let us consideri, at the same temperature, two chemically identical chains of length L_1 and L_2, respectively, and their CGRs in terms of n_1 and n_2 blobs, each blob consisting of the same number m of monomers. If we assume that (i) the size of the blob is the same for the two chains (this hypothesis looks reasonable, but we shall show below that it is only a rough approximation) and that (ii) interactions are independent on chemical distance except for very close blobs along the chain (again this looks quite plausible), we expect the potentials to be approximately transferable without any change as in the good-solvent case. However, since $z = (T - T_\theta)L^{1/2}$, the two chains correspond to two different crossover parameters z_1 and z_2. Therefore, the CGM with $n > 4$ blobs obtained by using the tetramer potentials at z is a CGM for a system at $z' > z$. In the renormalization-group language, z flows towards the stable good-solvent fixed point as the number of blobs increases. If hypotheses (i) and (ii) above were both approximately correct, we could simply estimate $z' = z(n/4)^{1/2}$. However, since $z' \neq z$, we expect $\hat{r}_g$ to differ in the two cases, hence hypothesis (i) does not hold, and therefore the relation between z and z' is more complex.

It is interesting to revisit this argument within the usual interpretation of the coarse-graining procedure, in

TABLE V: The transferability mapping: for each z (z_4) in the tetramer model (A_{2-4} is the corresponding second-virial combination) we report the value of z (z_{10}), the corresponding second-virial combination A_{2-10}, and the rescaling factor λ [see Eq. (35)] for the decamer model.

$n=4$		$n=10$		
z_4	A_{2-4}	z_{10}	A_{2-10}	λ
$z^{(1)}=0.056215$	0.993	$z^{(10-1)}=0.08628$	1.374	0.9875
$z^{(2)}=0.148726$	1.978	$z^{(10-2)}=0.22953$	2.524	0.9833
$z^{(3)}=0.321650$	2.962	$z^{(10-3)}=0.47018$	3.442	0.9684
$z^{(4)}=0.728877$	3.943	$z^{(10-4)}=1.00862$	4.267	0.9604
$z^{(5)}=2.508280$	4.915	$z^{(10-5)}=3.74117$	5.088	0.9778

which an increase of n corresponds to an increase of the resolution of the polymer CGR. In this case z is fixed. The previous argument implies that potentials should become increasingly softer as the resolution increases, i.e., the effective z decreases with increasing n. This result is completely consistent with the general argument of deGennes,[2] who noted that, close to the θ point, polymers show two different spatial regimes. If we indicate with R_t the thermal blob size,[2] blobs such that $\hat{r}_g \ll R_t$ behave as ideal chains, while excluded-volume effects dominate for $\hat{r}_g \gg R_t$. For $\hat{r}_g \sim R_t$, which is the relevant case here, blobs behave in an intermediate way, excluded-volume effects becoming increasingly less relevant — hence the effective z decreases — as $\hat{r}_g$ decreases, i.e. when the resolution (number of blobs n) increases.

Given the difficulties presented above, we have developed a transferability procedure which works at a formal level, without any explicit reference to the underlying polymer system. The idea is the following. Consider the tetramer set of potentials $\{V_4\}$ at a given value of z, $z = z_4$, and a system of $n > 4$ blobs interacting with these potentials. The question we will ask is: can this n-blob system be seen as a CGR of a polymer chain at a different value of z, say z_n? As we shall show below, the answer is positive. We will compute z_n and we will relate the size of the new CGR, i.e. $\hat{R}_{g,b}$, to the size of the corresponding underlying polymer chain. In terms of the underlying model, the tetramer potentials appropriate to describe a polymer chain at temperature T can be transferred without changes to an n blob CGR of the same polymer chain, but at a different temperature $T' > T$. In the renormalization-group (RG) language, we are considering a RG transformation at fixed *bare* parameters, hence we must consider the temperature RG flow towards the good-solvent fixed point $T = \infty$.

B. Definition of the higher-resolution models

Our recipe to transfer the tetramer potentials to n-blob CGMs works as follows. First, we introduce two universal functions: We define $F_{A,b}(A_2, n) = B_2(z)/[\hat{R}_{g,b}(z, n)]^3$ [B_2 is the second virial coefficient defined in Eq. (1)], which is a universal function of z and n or, equivalently, of A_2 and n, and $S_b(A_2, n) = \hat{R}_{g,b}(z, n)/\hat{R}_g(z)$ which is also a universal function of A_2 and n. Of course, the two functions are related by $F_{A,b}(A_2, n) = A_2 S_b(A_2, n)^{-3}$. These two functions can be computed by FM simulations and are assumed known in the procedure we shall present. For $n = 10$, the case we will be interested in, they are reported in Appendix A.

The procedure is the following:

(i) We consider the n-blob model with the same potentials used for the tetramer. For the bonding potentials we set $V_{ij}(\rho; n) = V_{ab}(\rho; 4)$, where ij are related to ab as in Eq. (33), while angular potentials are unchanged. No rescalings are performed at this stage, so that ρ for the n-blob model should not be identified with $r/\hat{R}_g$. We will write therefore $\rho = r/R$, where R simply sets the length scale but is otherwise arbitrary (in the numerical computations we set $R = 1$). Then, we compute (for instance, by Monte Carlo simulations) the second virial coefficient $B_{2,MC}$, the radius of gyration $\hat{R}_{g,b,MC}$, and $A_{2,b,MC} = B_{2,MC}/\hat{R}^3_{g,b,MC}$ of the n-blob chain.

(ii) We determine the value of A_2 appropriate for the n-blob model, i.e. $A_2(z_n, n)$, by solving the equation $F_{A,b}(A_2, n) = A_{2,b,MC}$. Then, using Eq. (4), we determine the n-blob corresponding z_n.

(iii) The radius of gyration $\hat{R}_g$ of the polymer chain, whose CGR is provided by the n-blob chain, is given by $\hat{R}_{g,MC} = \hat{R}_{g,b,MC}/S_b(A_2, n)$, using the value of A_2 computed at point (ii).

(iv) Once $\hat{R}_g$ is known, if we wish to express all lengths in terms of the radius of gyration, it is enough to redefine the bonding and the intermolecular potentials as

$$V(\rho'; z_n; n) = V(\rho' \hat{R}_{g,MC}/R; z; 4), \tag{34}$$

where $\rho' = r/\hat{R}_g(z_n; n)$.

With these definitions, we obtain a model with a higher resolution at a different value z_n, which has the correct A_2, hence it gives the correct thermodynamics, and gives the correct result for $\hat{R}_{g,b}(z; n)/\hat{R}_g(z; n)$, hence it is also structurally consistent.

We have applied this strategy starting from the tetramer potentials at $z = z^{(1)}, \ldots, z^{(5)}$. For each of them we have determined a decamer model with $n = 10$ blobs. The corresponding values of z_{10} and $A_2(z_{10})$ are reported in Table V. To clarify the procedure, let us show how the method works in a specific example, applying the transferability procedure to the tetramer model at $z = z^{(1)} = 0.056215$ (Explicit expressions for the corresponding potentials are reported in the supplementary material[36]). Consider the decamer model with $n = 10$, using the tetramer potentials (no rescalings are

performed). For this model we determine numerically [point (i)] $B_{2,MC}R^{-3} \approx 5.740$, $\hat{R}_{g,b,MC}/R \approx 1.532$, and $A_{2,b,MC} \approx 1.597$. Then [point (ii)], we first solve the equation $F_{A,b}(A_2, 10) = 1.597$ ($F_{A,b}(A_2, 10)$ is given in App. A), obtaining $A_2 \approx 1.375$, and then the equation $A_2(z_{10}) = 1.375$ [$A_2(z)$ is given in Eq. (4)], obtaining $z_{10} \approx 0.0862$. For such value of A_2, the results of App. A give $S_b(A_2, 10) \approx 0.951$, hence $\hat{R}_{g,MC}/R \approx 1.610$. Hence, for the decamer model, if we set $\rho' = r/\hat{R}_g$ expressing all lengths in terms of the radius of gyration of the underlying polymer chain, we should rescale the potentials as $V(\rho'; 10) = V(1.61\rho'; 4)$. In the good-solvent case, the rescaling is equal to the ratio $\mathcal{R}_4/\mathcal{R}_n = \hat{r}_{g,4}/\hat{r}_{g,n}$. In the crossover region, this relation does not hold, because of the flow of z. Hence we define

$$\lambda = \frac{\hat{r}_g(z_4, 4)}{\hat{r}_g(z_4, n)} \frac{R}{\hat{R}_{g,MC}}, \tag{35}$$

which encodes how much of the length rescaling is due to the change of the parameter z. At the renormalization-group fixed points $z = 0$ and $z = \infty$, we have $\lambda = 1$. In the example presented above we have $\hat{r}_g(z_4, 4)/\hat{r}_g(z_4, n) \approx 1.590$, so that $\lambda \approx 0.988$. The correction is small but not negligible.

As we discussed in Sec. V A, a naive application of the transferability ideas would predict $z_n = z_4(n/4)^{1/2}$. We can check how this approximation works in the present case. If we set $z_{10} = z_4(10/4)^{1/2}$, for our five values of z_4 we would obtain $z_{10} = 0.0889, 0.235, 0.506, 1.15, 3.97$, which are close to the estimates reported in Table V.

C. Comparison with full-monomer results

By definition, our procedure is such that A_2 and the ratio $\hat{R}_{g,b}/\hat{R}_g$ at zero density are exactly reproduced. We wish now to check whether other structural and thermodynamic properties are satisfied. In Figs. 12 and 13 we show the zero-density intramolecular distribution function $g_{\rm intra}(\rho)$ and the distribution of the CGR radius of gyration $\hat{R}_{g,b}$, respectively. In both cases, the agreement is excellent, confirming that the intramolecular structure is correctly reproduced. In Fig. 14 we show the zero-density center-of-mass pair distribution function for the decamer and for the polymer chain: again, the decamer appears to be quite accurate. Note that all these results are far from obvious and indicate that our procedure has correctly identified the renormalization-group flow from the θ point to the good-solvent fixed point.

Let us now consider the thermodynamic behavior. By construction, the decamer model reproduces the second-virial combination A_2. Let us now consider the third virial combination $A_3 = B_3\hat{R}_g^{-6}$. In Table VI we report the results for the SB model, the tetramer, and the decamer model, and compare them with the FM predictions.[15] The SB model significantly underestimates A_3, as already observed in Sec. IV A. The tetramer model

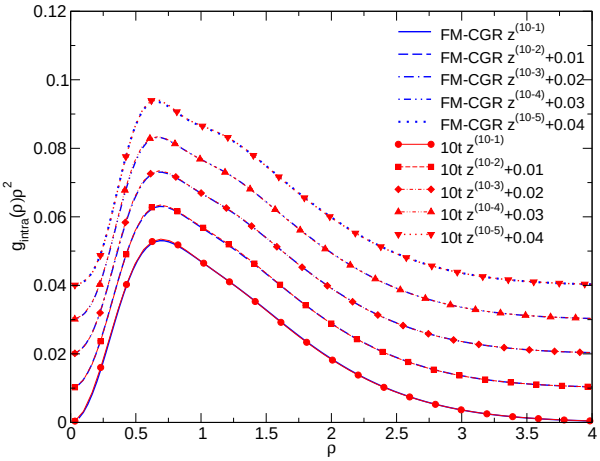

FIG. 12: Intramolecular distribution function $g_{\rm intra}(\rho)\rho^2$ at zero density as a function of $\rho = r/\hat{R}_g$. We report decamer (10t) and full-monomer (FM-CGR) results for several values of z, see Table V. For the sake of clarity, results at different values of z are shifted upward according to the legend.

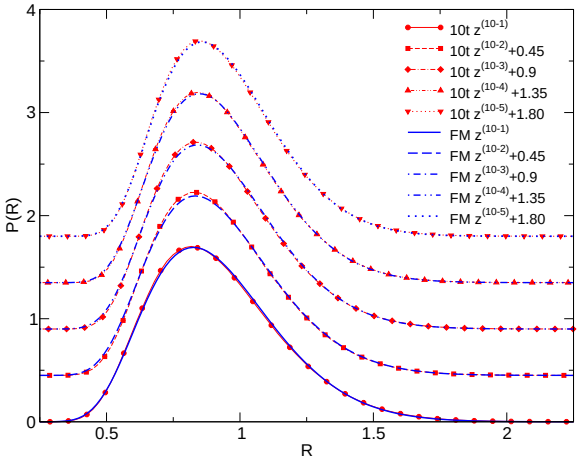

FIG. 13: Distribution of the ratio $R = \hat{R}_{g,b}/\sqrt{\hat{R}_g^2}$ at zero density. We report decamer (10t) and full-monomer (FM-CGR) results for several values of z, see Table V. For the sake of clarity, results at different values of z are shifted upward according to the legend.

appears to be accurate close to the good-solvent limit, but some deviations are observed for intermediate values of z. The decamer model reproduces the FM results with a relative accuracy of less than 1% for all values of z, hence 10 blobs are enough to reproduce quite accurately the thermodynamic behavior in the low-density regime.

Finally, let us consider the finite-density behavior. In the absence of FM simulations for $z^{(10-1)}$, ..., $z^{(10-5)}$, we cannot directly compare structural properties. We will thus limit ourselves to compare the thermodynamic

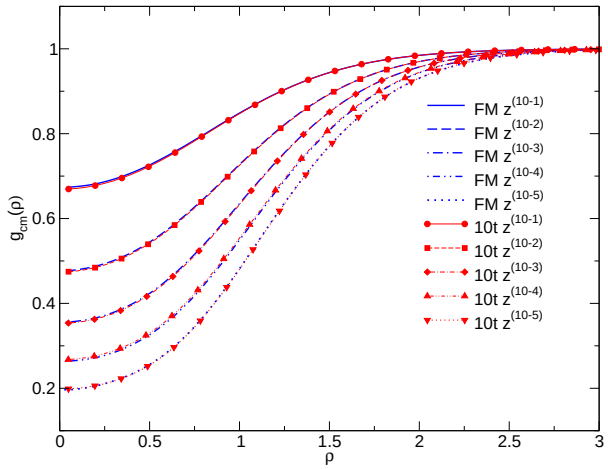

FIG. 14: Radial distribution functions for a pair of isolated chains as a function of the center-of-mass separation $\rho = r/\hat{R}_g$. We report decamer (10t) and full-monomer (FM) results at zero density for several values of z, see Table V.

TABLE VI: For several values of z, see Table V, we report A_3 for polymers (A_{3-FM}),[15] for the decamer (A_{3-10}), for the tetramer (A_{3-4}), and for the SB model A_{3-SB}.

z	A_{3-FM}	A_{3-10}	A_{3-4}	A_{3-SB}
$z^{(10-1)}$	0.216	0.217(1)	0.2042(6)	0.152
$z^{(10-2)}$	1.18	1.191(5)	1.132(4)	0.891
$z^{(10-3)}$	2.76	2.78(1)	2.540(6)	2.160
$z^{(10-4)}$	4.95	4.99(2)	4.91(1)	3.944
$z^{(10-5)}$	7.96	7.95(3)	7.94(1)	6.396

behavior, using the field-theory expressions[5] of App. B, to compute K as a function of Φ. As we discussed in Sec. IV B, field theory appears to be quite accurate, differences from the FM value being at most 4%. In Table VII we report $K(z,\Phi)$ for the different CGMs and compare it with the field-theory prediction. As expected, close to the θ-point ($z = z^{(10-1)}$), the decamer reproduces very precisely the polymer result, at least for $\Phi \leq 6$. To estimate the discrepancy for larger values of Φ [see Eq. (31)], we use the RPA estimates of the asymptotic behavior reported in Table VIII. Discrepancies appear to be under control for all values of Φ, being at most 6% in the limit $\Phi \to \infty$. For $z = z^{(10-3)}$ differences are reasonable up to $\Phi \lesssim 6$. For larger densities the systematic deviations are larger and Z and K are underestimated by 21% for $\Phi \to \infty$. For $z = z^{(10-5)}$ the behavior is similar to that observed in the good-solvent regime:[30] the decamer model is significantly more precise than the tetramer one and appears to be reliable up to $\Phi \approx 4$.

TABLE VII: Estimates of K for the CGM with $n = 4, 10$ blobs and for the single-blob (SB) model. For the polymer model we report the field-theory (FT) results of Ref. 5, see App. B. We also report the relative deviations $\Delta_n = 100|K_n/K_{FT} - 1|$ with respect to the field-theory result. Values of z reported in Table V.

z	Φ	FT	$n = 10$	$n = 4$	SB	$\Delta_{10}\%$	$\Delta_4\%$	$\Delta_{SB}\%$
$z^{(10-5)}$	1	4.45	4.42(2)	4.29(1)	3.91	0.7	3.6	12.1
	2	8.98	8.64(7)	8.135(25)	7.02	3.8	9.5	21.8
	4	19.56	17.9(2)	16.18(8)	13.26	8.5	17.3	32.2
	6	31.30	27.5(5)	23.9(3)	19.49	12.1	23.6	37.7
$z^{(10-3)}$	1	2.99	2.965(4)	2.85(1)	2.83	1.0	4.7	6.35
	2	5.29	5.18(3)	4.98(1)	4.76	2.1	5.9	10.0
	4	10.23	10.00(6)	9.19(4)	8.64	2.2	10.2	15.5
	6	15.38	14.6(1)	13.8(2)	12.52	5.0	10.3	18.6
$z^{(10-1)}$	1	1.69	1.686(9)	1.685(4)	1.67	0.2	0.3	1.2
	2	2.41	2.42(2)	2.386(7)	2.36	0.4	1.0	2
	4	3.89	3.91(3)	3.80(2)	3.75	0.5	2.3	3.6
	6	5.39	5.33(8)	5.28(7)	5.15	1.1	1.9	4.7

TABLE VIII: RPA coefficients $k_{SB}(z)$ and $k_n(z)$, and corresponding full-monomer coefficient $k_{FM}(z)$; see Sec. IV D for the definitions. We also report the relative deviations $\Delta_{10} = 100|k_{10}(z)/k_{FM}(z) - 1|$ for the decamer. Values of z reported in Table V.

z	$k_{SB}(z)$	$k_4(z)$	$k_{10}(z)$	$k_{FM}(z)$	$\Delta_{10}(z)\%$
$z^{(10-1)}$	0.698	0.727	0.751	0.798	6%
$z^{(10-2)}$	1.357	1.469	1.563	1.798	13%
$z^{(10-3)}$	1.937	2.201	2.397	3.042	21%
$z^{(10-4)}$	2.502	2.976	3.339	4.990	33%
$z^{(10-5)}$	3.103	3.922	4.587	10.39	56%

VI. CONCLUSIONS

Recently,[29,30] we developed a consistent coarse-graining strategy for polymer solutions under good-solvent conditions. In this work we extend this strategy to the thermal crossover region. For large values of L, the universal features of the thermal crossover can be completely characterized in terms of universal scaling functions, which can be conveniently computed[18] by using the two-parameter model (TPM), at least not too close to the θ point. Taking advantage of this relation, full-monomer results have been obtained by performing simulations of the Domb-Joyce model,[21] which represents the lattice version of the TPM. The TPM results are obtained by varying the on-site repulsion parameter w together with the chain length L, in such a way to keep the product $wL^{1/2}$ fixed when taking the scaling limit $L \to \infty$. This procedure enables us to explore the thermal crossover region at fixed $z = (T - T_\theta)L^{1/2}$ and re-

duced density Φ and, therefore, provides predictions for the scaling functions associated with any generic property of the solution.

TPM zero-density scaling functions are used as target distributions to develop a CG model. As in our previous investigation for chains in the good-solvent regime, we have first developed a tetramer model, that is a model in which each chain is represented by four "blobs." For the tetramer model we determine the interaction potentials at five different values of the parameter z, that correspond to different solvent quality. The intramolecular potentials are defined in such a way to reproduce the structure of an isolated chain. For this purpose we compute several single-chain scalar structural distributions and then use the iterative Boltzmann inversion procedure to determine the intramolecular potentials. Intermolecular interactions are specified by a single blob-blob pair potential which is determined by matching the radial distribution function between the centers of mass of the chains. The tetramer CG model set up at zero density is found to reproduce the collective behavior at finite density reasonably well up to a density $\tilde{\Phi}(z)$ which decreases with increasing z. For small values of z, i.e., close to the θ regime, the tetramer model can be safely used up to very high Φ (the error on Z is at most 1% up to $\Phi \sim 10$), as long as L is large enough to avoid tricritical effects. On the other hand, close to the good-solvent regime, we recover our previous finding that the tetramer model is reliable up to $\tilde{\Phi} \sim 2$.

In order to enlarge the range of applicability of the CG model with density, we have also developed a transferability procedure which allows us to use the tetramer potentials to build CG models with more blobs per chain. While in the good-solvent regime a simple rescaling of the characteristic length scale of the tetramer potentials was found to be sufficient to provide models with higher CG resolutions, in the crossover regime we must both change the basic length scale and temperature, i.e., z, as the number of blobs is increased. Using this more elaborate procedure, we have transferred the tetramer potentials to a CG model with 10 blobs per chain. As expected, the density range in which the predictions of the decamer CG model are accurate is enlarged with respect to the tetramer case.

This work completes our effort to develop a CG strategy for polymer solutions which employs potentials derived at zero density, but which is still able to predict the correct thermodynamics and structural properties of the system at finite density, deep into the semidilute regime. Since the potentials are derived at zero density, we avoid all inconsistencies related to the use of state-dependent potentials,[31–33] which plague most of the CG models employed to study complex fluids. Our CG model can be used to investigate temperature effects in polymer solutions, hence to compare with experimental results obtained by using chains of limited extension and that lie in this intermediate region of the phase diagram. Extensions of our strategy to treat polymer-wall and polymer-colloid interactions, polymers of different architecture, and copolymers are under investigation and will open the way to a fully consistent CG modeling of more challenging and interesting systems such as polymer solutions of various solvent quality in the presence of an absorbing wall (depletion interactions), colloid-polymer solutions, and block copolymer solutions, the behavior of which is well characterized by experiments but not so well by theory.

Appendix A: The blob radius of gyration

TABLE IX: Estimates of the ratios $\hat{R}^2_{g,b}/\hat{R}^2_g$ for $n = 4$ and $n = 10$ blobs for several values of z, see Table I.

z	$n = 4$	$n = 10$
0	0.7500	0.9000
$z^{(1)}$	0.7553(3)	0.9032(2)
$z^{(2)}$	0.7612(2)	0.9068(3)
$z^{(3)}$	0.7686(5)	0.9114(2)
$z^{(4)}$	0.7769(5)	0.9167(2)
$z^{(5)}$	0.7874(4)	0.9236(1)
∞	0.7959(2)	0.9295(2)

In this Appendix we wish to compute the function $S_b(A_2, n) = \hat{R}_{g,b}(z, n)/\hat{R}_g(z)$ for $n = 4$ and $n = 10$, which we parametrize in terms of A_2 instead of z. We first determine its behavior for $A_2 \to 0$, by performing a one-loop computation in the two-parameter model.[4,5] We begin by considering the average quadratic distance between monomers i and j. If L is the total number of monomers of the chain, i.e. its contour length, $x = i/L$ and $y = j/L$, we have for $j > i$:

$$\frac{1}{\hat{R}^2_{g,0}}\langle(\mathbf{r}_i - \mathbf{r}_j)^2\rangle = 6(y-x) + \frac{8}{3}z\Big[12xy^{1/2} - 8x^{3/2} - 4y^{3/2} + 8(y-x)^{3/2} + 3(x-y)^2 + 4(2+x-3y)\sqrt{1-x} - 8(1-y)^{3/2}\Big], \quad \text{(A1)}$$

where $\hat{R}^2_{g,0}$ is the radius of gyration for the ideal case ($z = 0$). We define the swelling factor associated with $\hat{r}_g$ as

$$\alpha_g(n, z) = \frac{\hat{r}^2_g(n, z)}{\hat{r}^2_g(n, 0)}. \quad \text{(A2)}$$

Using the expression reported above we obtain to first order in z:

$$\alpha_g(1, z) = 1 + \frac{134}{105}z, \quad \text{(A3)}$$

$$\alpha_g(2, z) = 1 + \frac{1}{105}(912\sqrt{2} - 1181)z = 1 + 1.036z, \quad \text{(A4)}$$

$$\alpha_g(3, z) = 1 + 0.914z, \quad \text{(A5)}$$

$$\alpha_g(4, z) = 1 + 0.833z. \quad \text{(A6)}$$

For $n \geq 5$, the large-n approximation

$$\alpha_g(n,z) = 1 + z\left(\frac{256}{105}\frac{1}{\sqrt{n}} - \frac{2}{n} + \frac{0.98}{n^{3/2}}\right), \qquad \text{(A7)}$$

works well. Since

$$S_b(A_2,n) = \frac{\hat{R}^2_{g,b}}{\hat{R}^2_g} = 1 - \frac{\hat{r}^2_g}{\hat{R}^2_g} = 1 - \frac{\hat{r}^2_{g,0}}{\hat{R}^2_{g,0}}\frac{\alpha_g(n,z)}{\alpha_g(1,z)}, \quad \text{(A8)}$$

We obtain for $z \to 0$

$$\begin{aligned} S_b(A_2,4) &= 0.75 + 0.110793 z = 0.75 + 0.00497423 A_2, \\ S_b(A_2,10) &= 0.90 + 0.067556 z = 0.90 + 0.00303304 A_2, \end{aligned} \qquad \text{(A9)}$$

where we used $z = 2A_2(4\pi)^{-3/2}$ to leading order. To obtain the behavior for all values of A_2, we use the results reported in Table IX, which have been obtained by FM simulations of the DJ model. Interpolating the data we obtain

$$\begin{aligned} S_b(A_2,4) &= \left(0.75 + 0.00497423 A_2 + 0.00023944 A_2^2 \right. \\ &\quad \left. + 0.0000679109 A_2^3\right)^{1/2}, \qquad \text{(A10)} \\ S_b(A_2,10) &= \left(0.9 + 0.00303304 A_2 + 0.000509387 A_2^2 \right. \\ &\quad \left. - 0.000153285 A_2^3 + 0.0000250389 A_2^4\right)^{1/2}. \end{aligned}$$

Given $S_b(n)$, we can then compute $F_{A,b}(n) = A_2/S_b(n)^3$.

Appendix B: Field-theory predictions

We summarize here the field-theoretical results of Schäfer,[5] reporting the basic formulae which allow one to compute the compressibility factor in terms of Φ and z. In this approach the crossover and density behavior is parametrized by two independent variables f and w. The variable f parametrizes the crossover from ideal ($f = 0$) to good-solvent behavior ($f = 1$), while w parametrizes the density dependence, $w = 1$ corresponding to $\Phi = 0$ and $w = 0$ to $\Phi = \infty$. To relate them to z and the polymer volume fraction Φ, we need to define several auxiliary functions (see Chap. 13 of Ref. 5):

$$\begin{aligned} H(f) &= 1 - 0.005 f - 0.028 f^2 + 0.022 f^3, \qquad \text{(B1)} \\ H_u(f) &= (1 + 0.824 f)^{0.25}, \qquad \text{(B2)} \\ H_n(f) &= H(f) H_u(f)^{-2}. \qquad \text{(B3)} \end{aligned}$$

Then, we define (Eqs. (13.27) and (15.12) of Ref. 5):

$$\begin{aligned} \alpha_g^2(f) &= (1-f)^{(1-2\nu)/\nu\omega} H(f)(1 - 0.195 f), \qquad \text{(B4)} \\ \tilde{z}(f,w) &= f(1-f)^{-1/(2\nu\omega)} H_n(f)^{-1/2}\sqrt{n_0}/w, \qquad \text{(B5)} \\ \tilde{s}(f,w) &= \frac{c_0 n_0}{\tilde{u}\tilde{z}(f,w)}(1-f)^{(3\nu-2)/\omega\nu} \\ &\quad \times H_u(f) H(f)^{-2}(1-w^2)/w^2, \qquad \text{(B6)} \end{aligned}$$

where $\tilde{u} = 8.1075$, $c_0 = 1.2$, $n_0 = 0.53$, $\nu = 0.588$, $\omega = 0.80$. Here α_g is the usual expansion factor, $\alpha_g = \hat{R}_g/\hat{R}_{g0}$, where $\hat{R}_{g0}$ is the value of the radius of gyration for the ideal chain, $\tilde{z}$ corresponds to the crossover variable z apart from a normalization ($z = 0.182\tilde{z}$), while $\tilde{s}$ is $cN^{3/2}$, where c is the concentration.

Given z and Φ, to obtain f and w we work as follows. First, we compute $\tilde{f}$ such that $\tilde{z}(\tilde{f},1) = z/0.182$ ($\tilde{f}$ and $w = 1$ correspond to z and $\Phi = 0$ in our variables) and

$$s_t = \frac{3\Phi}{4\pi}\alpha_g(\tilde{f})^{-3}. \qquad \text{(B7)}$$

Then, we determine f and w by solving the equations

$$\tilde{z}(f,w) = z/0.182 \qquad \tilde{s}(f,w) = s_t. \qquad \text{(B8)}$$

The compressibility factor is then determined as (Eqs. (17.21) and (17.51) of Ref. 5):

$$\begin{aligned} Z(f,w) &= 1 + \frac{1}{2}(1 + 2u^* f) W_R \\ &\quad - \frac{f u^* \sqrt{\pi N_R}}{3 W_R}\frac{0.808 + 1.22 W_R}{1 + 1.22 W_R} \\ &\quad \times \left[1 + (W_R - 1)(1 + 2W_R)^{1/2}\right], \end{aligned} \qquad \text{(B9)}$$

where $u^* = 0.364$, W_R and N_R are functions of w given by

$$W_R = c_0 n_0 (1 - w^2)/w^2 \qquad N_R = n_0/w^2. \qquad \text{(B10)}$$

* Electronic address: giuseppe.dadamo@aquila.infn.it
† Electronic address: andrea.pelissetto@roma1.infn.it
‡ Electronic address: carlo.pierleoni@aquila.infn.it

[1] P. Flory, *Principles of Polymer Chemistry* (Cornell University Press, Ithaca, NY, 1953).
[2] P. G. de Gennes, *Scaling Concepts in Polymer Physics* (Cornell University Press, Ithaca, NY, 1979).
[3] K. F. Freed, *Renormalization Group Theory of Macromolecules* (Wiley, New York, 1987).
[4] J. des Cloizeaux and G. Jannink, *Polymers in Solution: Their Modelling and Structure* (Clarendon, Oxford, 1990).
[5] L. Schäfer, *Excluded Volume Effects in Polymer Solutions*

(Springer Verlag, Berlin, 1999).
[6] In experimental work the low-density behavior of the osmotic pressure Π is usually written as $\Pi/(RT\rho) = 1/M + B_{2,\mathrm{expt}}\rho + O(\rho^2)$, where M is the molar mass of the polymer, ρ the weight concentration, and T the absolute temperature. Then, $B_2 \equiv M^2 B_{2,\mathrm{expt}}/N_A$, where N_A is the Avogadro number.
[7] M. Daoud and G. Jannink, J. Phys. (France) **37**, 973 (1976).
[8] P. G. de Gennes, Phys. Lett. **38A**, 339 (1972).
[9] N. Clisby, Phys. Rev. Lett. **104**, 55702 (2010).
[10] S. Caracciolo, B. M. Mognetti, and A. Pelissetto, J. Chem. Phys. **125**, 094903 (2006).
[11] P. Grassberger and R. Hegger, J. Chem. Phys. **102**, 6881 (1995); P. Grassberger, Phys. Rev. E **56**, 3682 (1995).
[12] B. Duplantier, J. Phys. (France) **43**, 991 (1982); **47**, 745 (1986); Europhys. Lett. **1**, 491 (1986); J. Chem. Phys. **86**, 4233 (1987); B. Duplantier and G. Jannink, Phys. Rev. Lett. **70**, 3174 (1993).
[13] J. Hager and L. Schäfer, Phys. Rev. E **60**, 2071 (1999).
[14] A. Pelissetto and J.-P. Hansen, J. Chem. Phys. **122**, 134904 (2005).
[15] S. Caracciolo, B. M. Mognetti, and A. Pelissetto, J. Chem. Phys. **128**, 065104 (2008).
[16] J. T. Titantah, C. Pierleoni, and J. P. Ryckaert, Phys. Rev. E **60**, 7010 (1999).
[17] B. G. Nickel, Macromolecules **24**, 1358 (1991).
[18] A. D. Sokal, Europhys. Lett. **27**, 661 (1994); (erratum) **30**, 123 (1995).
[19] H. Yamakawa, *Modern Theory of Polymer Solutions* (Harper–Row, New York, 1971).
[20] B. H. Zimm, W. H. Stockmayer, and M. Fixman, J. Chem. Phys. **21**, 1716 (1953).
[21] C. Domb and G. S. Joyce, J. Phys. C **5**, 956 (1972).
[22] F. Müller-Plathe, Chem. Phys. Chem. **3**, 754 (2002).
[23] D. Reith, M. Pütz, and F. Müller-Plathe, J. Comp. Chem. **24**, 1624 (2003).
[24] C. Peter and K. Kremer, Soft Matter **5**, 4357 (2009).
[25] H. A. Karimi-Varzaneh and F. Müller-Plathe, in *Multiscale Molecular Methods in Applied Chemistry*, edited by B. Kirchner and J. Vrabec, Top. Curr. Chem. **307** (Springer, Berlin, 2012), p. 295.
[26] H. Wang, C. Junghans, and K. Kremer, Eur. Phys. J. E **28**, 221 (2009).
[27] S. Izvekov and G. A. Voth, J. Phys. Chem B **109**, 2469 (2005); J. Chem. Phys. **123**, 134105 (2005); W. G. Noid, Methods Mol. Biol. **924**, 487 (2013).
[28] W. G. Noid, J. W. Chu, G. S. Ayton, and G. A. Voth, J. Phys. Chem. B **111**, 4116 (2007); J. W. Mullinax and W. G. Noid, Phys. Rev. Lett. **103**, 198104 (2009).
[29] G. D'Adamo, A. Pelissetto, and C. Pierleoni, Soft Matter **8**, 5151 (2012).
[30] G. D'Adamo, A. Pelissetto, and C. Pierleoni, J. Chem. Phys. **137**, 024901 (2012).
[31] F. H. Stillinger, H. Sakai, and S. Torquato, J. Chem. Phys. **117**, 288 (2002).
[32] A. A. Louis, J. Phys.: Condens. Matter **14**, 9187 (2002).
[33] G. D'Adamo, A. Pelissetto, and C. Pierleoni, *Predicting the thermodynamics by using state-dependent interactions*, submitted.
[34] T. P. Lodge, J. Bang, Z. Li, M. H. Hillinger, and Y. Talmon, Faraday Discuss. **128**, 1 (2005).
[35] I. W. Hamley, *Block Copolymers in Solution* (Wiley, Chichester, 2005).
[36] Supplementary material.
[37] W. J. C. Orr, Trans. Faraday Soc. **12**, 43 (1947).
[38] E. W. Montroll, J. Chem. Phys. **734**, 18 (1950).
[39] A. J. Barrett and C. Domb, Proc. Roy. Soc. London A **367**, 143 (1979).
[40] P. Belohorec and B.G. Nickel, "Accurate universal and two-parameter model results from a Monte-Carlo renormalization group study," Guelph University report, 1997 (unpublished).
[41] V. Krakoviack, J. P. Hansen, and A. A. Louis, Phys. Rev. E **67**, 041801 (2003).
[42] C. I. Addison, A. A. Louis, and J. P. Hansen, J. Chem. Phys. **121**, 612 (2004).
[43] M. Lal, Mol. Phys. **17**, 57 (1969).
[44] B. MacDonald, N. Jan, D. L. Hunter, and M. O. Steinitz, J. Phys. A **18**, 2627 (1985).
[45] N. Madras and A. D. Sokal, J. Stat. Phys. **50**, 109 (1988).
[46] A. D. Sokal, in *Monte Carlo and Molecular Dynamics Simulations in Polymer Science*, edited by K. Binder (Oxford University Press, Oxford, 1995).
[47] T. Kennedy, J. Stat. Phys. **106**, 407 (2002).
[48] N. Clisby, J. Stat. Phys. **140**, 349 (2010).
[49] W. Schommers, Phys. Rev. A **28**, 3599 (1983).
[50] M. Laso, H. C. Öttinger, and U. W. Suter, J. Chem. Phys. **95**, 2178 (1991)
[51] R. L. C. Akkermans and W. J. Briels, J. Chem. Phys. **114**, 1020 (2001); J. Chem. Phys. **115**, 6210 (2001).
[52] A. Pelissetto, J. Chem. Phys., **129**, 044901 (2008).
[53] S. Caracciolo, A. Pelissetto, and A. D. Sokal, J. Stat. Phys. **60**, 1 (1990).
[54] M. S. Causo, J. Stat. Phys. **108**, 247 (2002).
[55] J. P. Hansen and I. McDonald, *Theory of Simple Liquids*, 3rd ed. (Academic Press, Amsterdam, 2006)
[56] J. L. Lebowitz and J. K. Percus, Phys. Rev. **124** 1673 (1961); L. R. Pratt and S. W. Haan, J. Chem. Phys. **74**, 1864 (1981); K. W. Kratky, J. Stat. Phys. **38**, 379 (1985); J. J. Salacuse, A. R. Denton, and P. A. Egelstaff, Phys. Rev. E **53**, 2382 (1996).
[57] C. Pierleoni, B. Capone, and J. P. Hansen, J. Chem. Phys. **127**, 171102 (2007).